https://doi.org/10.5194/egusphere-2026-6613
Preprint. Discussion started: 3 November 2026
© Author(s) 2026. CC BY 4.0 License.

Ocean Heat Content Estimates from Ocean Reanalyses since 1993

Haohao Zhang[1], Andrea Storto[2], Lijing Cheng[1], Romain Bourdallé-Badie[3], Satoshi Osafune[4], Andrea Cipollone[5], Caihong Wen[6], James A. Carton[7], Gaël Forget[8], Yuying Pan[1], Marie Drevillon[3], Karina von Schuckmann[3], Magdalena A. Balsamda[9], Matthew A. Chamberlain[10], Chunxue Yang[*2]

[1]State Key Laboratory of Earth System Numerical Modeling and Application, Institute of Atmospheric Physics, Chinese Academy of Sciences, Beijing 100029, China

[2]Institute of Marine Sciences (ISMAR), National Research Council of Italy (CNR), Via del Fosso del Cavaliere 100, 00133 Rome, Italy

[3]Mercator Ocean International, Toulouse, France

[4]Research Institute for Global Change (RIGC), Japan Agency for Marine-Earth Science and Technology (JAMSTEC), Yokosuka 237-0061, Japan

[5]CMCC Foundation—Euro-Mediterranean Center on Climate Change, Bologna, Italy

[6]Climate Prediction Center, National Centers for Environmental Prediction, National Weather Service, NOAA, College Park, MD 20740, USA

[7]Department of Atmospheric and Oceanic Science, University of Maryland, College Park, MD 20742, USA

[8]Department of Earth, Atmospheric and Planetary Sciences, Massachusetts Institute of Technology, Cambridge, MA 02139, USA

[9]Research Department, European Centre for Medium-Range Weather Forecasts (ECMWF), Reading, United Kingdom

[10]CSIRO Environment, Hobart, TAS, Australia

Correspondence to: Chunxue Yang (chunxue.yang@cnr.it)

https://doi.org/10.5194/egusphere-2026-6613
Preprint. Discussion started: 3 November 2026
© Author(s) 2026. CC BY 4.0 License.



Abstract.

Ocean heat content (OHC) is a key indicator of Earth's energy imbalance and long-term climate change. Within the Marine Environment Reanalyses Evaluation Project (MER-EP), we use recent-generation ocean reanalysis products (ORAs) to assess long-term global OHC changes, spatial warming patterns, and inter-product consistency since 1993. We compare the results with those from objective analysis products (OAs) and earlier-generation ORAs. The results show sustained global ocean warming during 1993–2022, concentrated mainly in the upper 2000 m. The ORA ensemble gives a global 0–2000 m OHC trend of 0.73 [0.49, 0.97] W m^{-2} ($\pm$1.65 std), with trend estimates from the OAs falling within the ORA uncertainty range. Warming is more pronounced at mid-to-high latitudes and extends to greater depths at high northern latitudes. Differences among ORAs are largest in the polar oceans, western boundary current regions, frontal systems, and below 2000 m. Inter-product consistency among ORAs improves markedly in the Argo era. In the upper 2000 m, the fraction of ocean area where the common ORA signal exceeds inter-product spread (signal-to-noise ratio > 1) increases by 20.8 percentage points for interannual variability and 21.3 percentage points for long-term trends after 2005. The largest improvement occurs in the 700–2000 m layer. Below 2000 m, inter-product consistency among ORAs remains low throughout the study period. Compared with earlier-generation ORAs, recent-generation ORAs also show a clear improvement in inter-product consistency for both interannual variability and long-term trends in upper-ocean OHC. These results increase confidence in using recent-generation ORAs to estimate global OHC changes and indicate that sustained ocean observations provide an essential foundation for reliably estimating global OHC changes.

https://doi.org/10.5194/egusphere-2026-6613
Preprint. Discussion started: 3 November 2026
© Author(s) 2026. CC BY 4.0 License.

1 Introduction

The ocean is the dominant heat reservoir in the Earth system because of its large heat capacity, as most of the excess heat associated with anthropogenic climate change is stored in the ocean (von Schuckmann et al., 2020). Global ocean heat content (OHC) has increased substantially since the 1960s, with the warming accelerating in recent decades, as consistently indicated by closely agreeing observation-based estimates and ocean reanalyses (Cheng et al., 2022; Minière et al., 2023; Storto and Yang, 2024). Ocean warming affects the climate system and the marine environment through thermosteric sea-level rise, marine heatwaves, stronger upper-ocean stratification and polar sea-ice decline (Cheng et al., 2022; Fox-Kemper et al., 2021; von Schuckmann et al., 2024). Therefore, accurate estimates of global and regional OHC, together with well-quantified uncertainties, are essential for monitoring the marine environment and climate system changes (von Schuckmann et al., 2024).

OHC estimates can be derived from several complementary types of data and methods. Objective analyses (OA) are observation-based but model independent gridded temperature products constructed from in situ measurements using statistical mapping and bias-correction methods. Examples include EN4, NCEI, Ishii, and IAP (Cheng et al., 2024; Good et al., 2013; Ishii et al., 2017; Levitus et al., 2012). Indirect and data-driven approaches, based on satellite/geodetic observations and machine-learning methods, also provide useful estimates of OHC changes, especially for assessing poorly observed deep-ocean warming and its uncertainty (Marti et al., 2022; Meyssignac et al., 2019; Storto et al., 2022; Su et al., 2020). Ocean reanalyses products (ORAs) provide another major source of OHC estimates by combining dynamical numerical models with observations through data assimilation, which can provide spatially and temporally continuous ocean states constrained by both observations and model dynamics (Balmaseda et al., 2013b; Storto et al., 2019; Yang et al., 2025). Different ORAs typically assimilate the same in situ data, but often amongst many other data sources, including from remote sensing, and add dynamical constraints provided by theory as encoded in the general circulation model's equations (Forget, 2010; Forget et al., 2015a; Forget and Ponte, 2015).

An early multi-product assessment by Xue et al., (2012) compared upper ocean OHC variability across an ensemble of operational ocean analyses and reanalyses. Since then, ORAs have been increasingly used

https://doi.org/10.5194/egusphere-2026-6613
Preprint. Discussion started: 3 November 2026
© Author(s) 2026. CC BY 4.0 License.

to quantify OHC variability and long-term ocean warming (Balmaseda et al., 2013a; Hakuba et al., 2024; Liu et al., 2024; Storto and Yang, 2024), ocean heat transport and regional heat redistribution (Forget and Ferreira, 2019; Jiang et al., 2026; Liu et al., 2024; Song and Forget, 2026), Earth's energy imbalance (Balmaseda et al., 2013a; Forget, 2026; Hakuba et al., 2024) and to evaluations of sea-level and ocean-mass budget closure (Bouih et al., 2025; Ludwigsen et al., 2024). However, OHC estimates from ORAs are affected by model biases, data-assimilation choices, atmospheric forcing uncertainties, as well as the sparse and time-varying distribution of observations. Different production centres use different ocean models, forcing fields, assimilation schemes and bias-correction methods (Forget et al., 2015a; MacLachlan et al., 2015; Menemenlis et al., 2008; Osafune et al., 2015; Storto et al., 2016). As a result, OHC estimates from ORA may differ across products, especially during periods and in regions where observational constraints are sparse or ocean dynamics are complex (Palmer et al., 2017).

Since the mid-2000s, the Core Argo array has greatly improved the coverage of upper-2000 m temperature and salinity observations, providing direct constraints for both OAs and ORAs (Johnson et al., 2022; Riser et al., 2016; Wong et al., 2020). The Argo system is also complemented by other instrumental systems such as ship-based hydrological observations, mooring buoys and gliders. Observing-system experiments with the ECMWF ocean reanalyses ORAS5 (Zuo et al., 2019) show that Argo observations strongly constrain upper-ocean temperature variability, as their removal increased the normalized RMSD of upper-700 m temperature interannual anomalies across much of the ocean during 2005–2015. From an observation-based OHC perspective, Zhu et al., (2026) showed that randomly removing 20 to 80% of GOOS observations increased the relative error in annual ocean heating rates from 33 ± 6% to 97 ± 20%, with even larger errors when data loss was spatially uneven. These results show that the observations are critical for constraining OHC estimates. Earlier studies had already suggested that the expansion of ocean observations improved agreement among ORAs. Xue et al., (2012) found that the spread of 0–300 m OHC estimates across operational ocean analyses and reanalyses generally decreased with time and reached a minimum as Argo observations became available. Palmer et al., (2017) also showed that agreement among ORAs weakened substantially with depth, with deep-ocean OHC remaining poorly constrained. However, both assessments were based on earlier-generation systems and

https://doi.org/10.5194/egusphere-2026-6613
Preprint. Discussion started: 3 November 2026
© Author(s) 2026. CC BY 4.0 License.

did not quantify how changes in inter-product agreement across the Argo transition varied among depth layers and regions. Whether the improvement persists in recent-generation ORAs, particularly below 300 m and outside well-observed regions, therefore remains unclear.

Over the past decade, the role of ocean reanalyses in major climate assessments has evolved. They were not used for evaluation in IPCC AR5 because many reanalyses properties depend on the underlying model system (Flato et al., 2013), whereas in AR6, improvements in ocean reanalyses were recognized. These improvements included advances in model physics, model resolution, data assimilation, and atmospheric forcing (Heimbach et al., 2019; Lellouche et al., 2018, 2021; Storto et al., 2019; Zuo et al., 2017). Nevertheless, reanalyses-based OHC estimates were not the primary products used to show OHC changes in AR6 (Fox-Kemper et al., 2021). Since then, ORAs have been increasingly used in global and regional OHC studies and operational marine climate monitoring, including Copernicus Marine indicators and the Copernicus Ocean State Report (Balmaseda et al., 2013a; Copernicus Marine Service, 2025; Forget, 2026; Hakuba et al., 2024; Jackson et al., 2019; Jiang et al., 2026; Liu et al., 2024; von Schuckmann et al., 2024; Song and Forget, 2026). Many current ORAs now extend more than a decade beyond the period covered by ORA-IP, providing longer common records and a potentially more robust basis for assessing long-term OHC changes and inter-product consistency. These methodological advances, broader applications, and longer time series motivate a reassessment of recent-generation ORAs for OHC monitoring.

This study, within the Marine Environment Reanalyses Evaluation Project (MER-EP; Yang et al., 2026, submitted), uses 13 recent-generation ORAs with 4 OAs for comparison, to examine whether ORA-based OHC estimates of trends and variability have become more consistent across the Argo deployment transition. We aim to address four questions: first, do ORAs and OAs show consistent large-scale OHC changes? Second, how does inter-ORA agreement change across the transition to the Argo era? Third, where do substantial ORA uncertainties remain as a function of depth and region? Fourth, has the consistency of the new-generation reanalyses data improved in comparison to the previous-generation reanalyses datasets, such as those included in ORA-IP?

https://doi.org/10.5194/egusphere-2026-6613
Preprint. Discussion started: 3 November 2026
© Author(s) 2026. CC BY 4.0 License.

2 Data and Methods

2.1 Datasets

The 13 ORAs and 4 OAs used in this study are listed in Table 1. This study also uses two observation-based time series for comparison: the Global Estimates of Ocean Heat Content (GOHC) ensemble mean (Minière et al., 2026) and the Global Climate Observing System (GCOS) OHC (von Schuckmann et al., 2023). The comparison between ORAs and OAs is used to assess product consistency, not to estimate the true state of the ocean, because the OAs are also affected by observational sampling, XBT/MBT bias correction, reference climatology, and mapping methods (Boyer et al., 2016; Cheng et al., 2024; Liang et al., 2021; Yuan et al., 2026).

In this study, we focus on four fixed depth ranges: 0–700 m, 700–2000 m, 0–2000 m, and 2000–5000 m. The trend analysis is based on the 30-year period 1993–2022, and the diagnostic regions include both the global ocean and the latitude range of 60°S–60°N. Of the 13 ORAs, eight products are used consistently to calculate the ORA ensemble mean (ORA EM), ensemble spread and signal-to-noise ratio (S/N) analysis. BRAN2020, ESTOC, and GODAS are excluded from these ensemble-based diagnostics because they do not cover the full global ocean, while GloSia9-1 is excluded because it ends in 2020 and therefore does not cover the full 1993–2022 analysis period. In addition, although GLORYS12v1 meets both the temporal and spatial requirements, compared to all ORAs and OAs used in this study, this dataset shows a marked rapid increase in OHC after approximately 2019 and include it in the ensemble mean would also result in a significant increase in uncertainty after about 2019 (Fig. S1). Therefore, we consider it an outlier dataset. The new generation GLORYS12v2 is under production and will be evaluated when it is available. These five products are still retained as individual products and are compared with the individual OAs and ORAs.

For the spatial comparisons of OHC trends, we compare the ORA EM separately with each of the four OAs over their available depth ranges, rather than with the OA EM. IAPv4 provides OHC fields from the surface to 6000 m on 119 vertical levels and uses an updated objective-analysis framework (Cheng et al., 2024). EN4 is the only other OA used here that extends beyond 5000 m (Good et al., 2013). Ishii and

https://doi.org/10.5194/egusphere-2026-6613
Preprint. Discussion started: 3 November 2026
© Author(s) 2026. CC BY 4.0 License.

NCEI cover only the upper 3000m and 2000 m, respectively (Ishii et al., 2017; Levitus et al., 2012). An OA EM would therefore include four products in the upper 2000 m but only IAPv4 and EN4 in the 2000–5000 m layer. Its composition would change with depth, making comparisons across layers harder to interpret. With only two to four OAs available, their average could be sensitive to an individual product and obscure differences between the ORA EM and each OA product.

To assess whether the ORAs used in MER-EP show improved OHC consistency relative to earlier-generation ORAs, we also used the Ocean Reanalyses Intercomparison Project (ORA-IP) data analysed by Palmer et al., (2017) and compared them with the eight-member ORA ensemble used in MER-EP. The comparison was restricted to 1993–2010, because most ORA-IP ORAs end in or near 2010, and 12 ORA-IP ORAs provide global coverage over this period, namely CFSR, C-GLORS, ECCOJPL, ECDA, GECCO2, GloSea5, GODAS, K7, MOVEC, MOVEG2, SODA and UoR (more detail shown in Palmer et al., 2017 Table1). The comparison with ORA-IP focuses on the 0–1500 m layer, as ORA-IP does not provide 0–2000 m OHC fields.

https://doi.org/10.5194/egusphere-2026-6613
Preprint. Discussion started: 3 November 2026
© Author(s) 2026. CC BY 4.0 License.

175 **Table 1. Overview of the different objective analysis and reanalyses products used in MER-EP.**

Product	Institution	Code version	Resolution	Latitude	Year used	Assimilation method	Reference
Objective Analysis products							
IAPv4	IAP/CAS		1°; 119 levels to 6000 m	Global	1993-2024	EnOI-DE	Cheng et al., (2024)
EN4	Met Office Hadley Centre		1°; 42 levels to 5350 m	Global	1993-2024	OI	Good et al., (2013)
Ishii	MRI/JMA		1°; 28 levels to 3000 m;	Global	1993-2024	3DVAR OA	Ishii et al., (2017)
NCEI	NOAA		1°; 26 levels to 2000 m	Global	1993-2024	Barnes OA	Levitus et al., (2012)
GOHC	Mercator Ocean		time series only	60°S-60° N	1993-2024		Minière et al., (2026)
GCOS	Mercator Ocean		time series only	60°S-60° N	1993-2020		von Schuckmann et al., (2023)
Reanalyses products							
C-GLORSv7	CMCC	NEMO3.4	1/4°; 75 levels to 5902 m	Global	1993-2024	OceanVar 3DVAR-FGAT	Storto et al., (2016)
C-GLORSv8	CMCC	NEMO4.2	1/4°; 75 levels to 5902 m	Global	1993-2023	OceanVar 3DVAR-FGAT	Selivanova et al., (2026)
CIGAR025	CNR-ISMAR	NEMO4	1/4°; 75 levels to 5902 m	Global	1993-2024	3DVAR + LSBC	Storto and Yang, (2024)
CIGAR1	CNR-ISMAR	NEMO4	1°; 75 levels to 5902 m	Global	1993-2024	3DVAR + LSBC	Storto and Yang (2024)
GLORYS2v4	MOI	NEMO3.1	1/4°; 75 levels to 5902 m	Global	1993-2024	SAM2-SEEK	Lellouche et al., (2013)
GLORYS4v2	MOI	NEMO3.6	1/4°; 75 levels to 5902 m	Global	1993-2023	SAM multiv. DA	Bourdallé-Badie et al., (2026)
ORAS5	ECMWF	NEMO3.4	1/4°; 75 levels to 5902 m	Global	1993-2024	NEMOVAR 3DVAR-FGAT	Zuo et al., (2019)
SODA3	University of Maryland	MOM5	1/4°; 50 levels to 5395 m	Global	1993-2024	SeqDA	Carton et al., (2018)
GLORYS12v1	MOI	NEMO3.1	1/12°; 50 levels to 5728 m	Global	1993-2024	SAM2 ROKF/3DVAR	Lellouche et al., (2021)
GloSia9-1	UK Met Office	NEMO3.4	1/4°; 75 levels to 5902 m	Global	1993-2020	NEMOVAR DA	Guiavarc'h et al., (2025)
BRAN2020	CSIRO	MOM5	1/10°; 51 levels to 4509 m	74.5°S-75° N	1993-2023	EnKF-C EnOI	Chamberlain et al., (2021)
ESTOC	JAMSTEC	MOM3	1°; 46 levels to 5525 m	74.5°S-79.5° N	1993-2022	Adjoint 4DVAR	Osafune et al., (2015)
GODAS	NOAA	MOM.v3	0.3°-1°; 40 levels to 4478 m	74.5°S-64.5° N	1993-2024	3DVAR	Huang et al., (2008)

https://doi.org/10.5194/egusphere-2026-6613
Preprint. Discussion started: 3 November 2026
© Author(s) 2026. CC BY 4.0 License.

2.2 Ocean heat content calculation

Because the products differ in temporal, horizontal, and vertical resolution (Table 1), all monthly temperature and salinity fields were linearly interpolated onto the native IAPv4 grid, with 1° × 1° horizontal resolution and 119 vertical levels, before OHC was calculated. This grid is used because IAPv4 provides full-depth fields and is one of the main OAs used for the spatial and vertical comparisons in this study, as mentioned in Section 2.1. To evaluate the sensitivity of global OHC estimates to spatial interpolation, we compared OHC calculated on the native grids of C-GLORSv8, GLORYS12v1, and ESTOC with the corresponding estimates after interpolation to the IAP grid. These products represent three distinct native-grid configurations: a curvilinear grid, a high-resolution regular grid, and a lower-resolution regular grid, respectively. The comparison results indicate that the impact of interpolation on global OHC is minimal (Fig. S2).

OHC contained in a given depth layer was calculated by vertically integrating conservative temperature from z_1 to z_2 (Cheng et al., 2024; Pan et al., 2023):

$$OHC = \int_{Z_1}^{Z_2} \rho C_p T dz \qquad (1)$$

where Z_1 and Z_2 are the upper and lower boundaries of the layer, respectively. The c_p is a constant of ~ 3991.9 J (kg K)$^{-1}$ used in TEOS-10 to define Conservative Temperature. ρ and T are the in-situ density (kg m^{-3}) and Conservative Temperature (°C), respectively. Both are calculated from absolute salinity, in-situ temperature, and sea pressure using International Thermodynamic Equation of Seawater–2010 (TEOS-10; Intergovernmental Oceanographic Commission et al., 2010).

Differences in product mean states and in the ocean volume represented by each product can affect absolute OHC values. Therefore, OHC anomalies are used for the time-series analyses and related statistics. For each product, the anomaly is calculated by subtracting that product's own annual mean OHC over the common 2005–2022 reference period (GCOS and GloSia9-1 are only available up to 2020, their reference period is 2005–2020).

https://doi.org/10.5194/egusphere-2026-6613
Preprint. Discussion started: 3 November 2026
© Author(s) 2026. CC BY 4.0 License.

In this study, the uncertainty in OHC estimates is represented using a 90% confidence interval (CI), or an approximate 90% CI. IAPv4 uncertainty is estimated from a 918-member observational ensemble that accounts for major sources of uncertainty, including data quality control, bias corrections, climatology, vertical interpolation, and sampling and mapping errors (Yuan et al., 2026) and its 90% CI is defined by the 5th and 95th percentiles of the ensemble distribution. For the GCOS, GOHC and eight-member ORA ensemble used in this study, an approximate 90% CI is calculated as the ensemble mean ± 1.65 times the sample standard deviation across ensemble members, assuming an approximately normal distribution. For EN4, Ishii, NCEI and individual ORA, no uncertainty range is shown.

2.3 Interannual-variability and trend signal-to-noise ratios

We calculated two complementary signal-to-noise ratios (S/N) to quantify cross-product consistency in OHC: one for detrended interannual variability and one for linear trends. Both diagnostics were calculated separately for the OAs and ORAs at each grid point and depth range. The primary analysis compared 1993–2004 (12 years) with 2005–2022 (18 years). To assess the robustness of this comparison using equal-length periods, both ORA diagnostics were additionally calculated for seven 12-year windows from 2005–2016 to 2011–2022. Each window was compared with 1993–2004. The OA S/N diagnostics included IAPv4, EN4, and Ishii. NCEI was excluded because of no annual gridded fields before 2005. The ORA calculation used the fixed eight-product ensemble mentioned in Section 2.1. Only the ORA results for 1993–2004 and 2005–2022 are presented in the main text; the OA results and the ORA sliding-window results are provided in the Supplementary Information.

For interannual variability, following Palmer et al. (2017), the signal was defined as the temporal sample standard deviation of the ensemble-mean detrended annual OHC time series. The noise was defined as the time average of the annual sample standard deviations across products. The interannual-variability S/N at each grid point and for each depth range was calculated as:

$$S/N = \frac{\sqrt{\frac{1}{T-1}\sum_{t=1}^{T}\left(\bar{H}'_t - \mu_{\bar{H}'}\right)^2}}{\frac{1}{T}\sum_{t=1}^{T}\sqrt{\frac{1}{M-1}\sum_{m=1}^{M}\left(H'_{m,t} - \bar{H}'_t\right)^2}} \quad (2)$$

https://doi.org/10.5194/egusphere-2026-6613
Preprint. Discussion started: 3 November 2026
© Author(s) 2026. CC BY 4.0 License.

Here, T is the number of years in the analysis period, and M is the number of products included in the ensemble. The $H'_{m,t}$ is the detrended value for product m in year t. The ensemble mean in year t is $\overline{H}'_t = \frac{1}{M}\sum_{m=1}^{M} H'_{m,t}$, and its temporal mean is $\mu_{\overline{H}'} = \frac{1}{T}\sum_{t=1}^{T} \overline{H}'_t$.

For trends, S/N was calculated as the absolute value of the ensemble-mean trend divided by the sample standard deviation of the trends across products:

$$S/N = \frac{|\overline{\beta}|}{\sqrt{\frac{1}{M-1}\sum_{m=1}^{M}(\beta_m - \overline{\beta})^2}} \quad (3)$$

where β_m is the slope obtained by fitting an ordinary least-squares regression to the annual OHC time series for product m over the analysis period, and $\overline{\beta} = \frac{1}{M}\sum_{m=1}^{M} \beta_m$ is the ensemble-mean trend.

Both S/N ratios are dimensionless. For interannual variability, an S/N value greater than one indicates that the temporal standard deviation of the ensemble mean exceeds the time-averaged inter-product spread. For trends, values greater than one indicate that the magnitude of the ensemble-mean trend exceeds the inter-product trend standard deviation. These diagnostics quantify the ensemble signal relative to inter-product spread.

3 Results

3.1 OHC time series and trend

The ORA EM and the OAs show broadly consistent large-scale OHC changes over the global ocean (Fig. 1). In the upper 700 and 2000 m, the ORA EM is generally lower than the OAs (Fig. 1). The increasing availability of Argo observations improved the constraint on OHC estimates in both the OAs and ORAs, thereby reducing the differences between the two kinds of datasets. After 2005, the ORA EM and OAs show closer agreement in the upper 2000 m, and the OAs analyzed here lie within the ORA inter-product spread. For the deep ocean 2000-5000 m layer, the ORA EM and IAPv4 agree well, although there is a large spread within the ORA ensemble. EN4 shows a slower deep warming trend than IAPv4 and ORA EM (Fig. 1d).

https://doi.org/10.5194/egusphere-2026-6613
Preprint. Discussion started: 3 November 2026
© Author(s) 2026. CC BY 4.0 License.

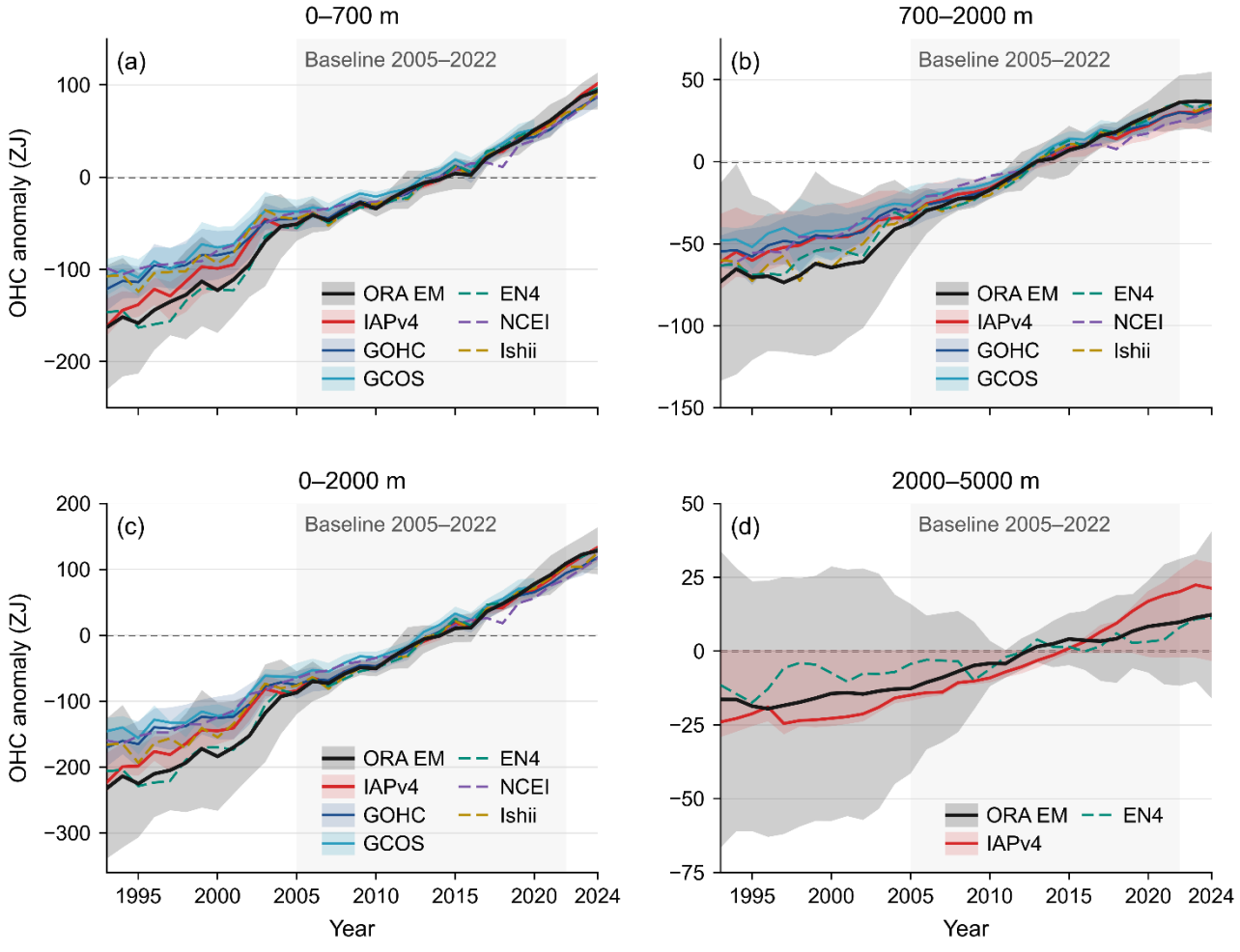
Here we use the ensemble spread of 8 ORAs (Fig. 1 light grey shaded area) as the uncertainty information because different reanalyses systems use different ocean models (e.g. model physics and schemes), data assimilation schemes, observations assimilated (beyond Argo that virtually all ORAs and OAs use) and atmospheric forcing, which could contribute the uncertainty coming from different components of the reanalyses (Yang et al., 2019). In terms of the OAs, we show the uncertainty information for the IAPv4 ensemble, GCOS and GOHC (von Schuckmann et al., 2023; Minière et al., 2026; Yuan et al., 2026). In general, ensemble spread in the upper 2000 m decreased substantially for both OAs and ORAs after 2005 as the Argo observing network expanded (Fig. 1c). Below 2000 m, both OAs and ORAs still exhibit large uncertainties relative to the small magnitude of warming, with greater uncertainties in ORAs (Fig. 1d). These happen because we have more observations in the upper ocean which constrain the ocean state but sparse observations in the deep layer. In the top 700 m, atmospheric forcing-driven ocean dynamics provides strong constraints to all ORAs which have a small spread relative to the other layers. In principle, we have more confidence for the upper ocean for example between 0–2000 m in particular post-Argo period, because of the strong atmospheric forcing and observational constraints but less confidence for the deep layer (below 2000m) where data are sparse and reanalyses are susceptible to model bias. In spite of the spread, there is consistency in the estimates of global and semi-global OHC between the ensemble mean of ORA and the OA at all depth levels.

Figure 2 compares the OHC trends of OAs and ORAs in 1993–2022. Most OAs and ORAs show positive OHC trends, with only a few exceptions in specific depth layers, indicating that sustained ocean warming since 1993 is a robust large-scale signal across OA and ORA product families. The ORA EM estimates an OHC trend of 0.73 [0.49, 0.97] W m^{-2} in the upper 2000 m over 1993–2022. The central estimates from IAPv4, EN4, Ishii, and GOHC are generally lower, at 0.65 [0.56, 0.70], 0.73, 0.61, and 0.55 [0.47, 0.64] W m^{-2}, respectively, but all fall within the ORA EM uncertainty range (Fig. 2c). The GOHC covers only 60°S–60°N (Minière et al., 2026), resulting in lower OHC trend estimates than those from the other global datasets. The globally integrated OHC trend is larger than the 60°S–60°N integrated trend, indicating a positive contribution from polar regions.

https://doi.org/10.5194/egusphere-2026-6613
Preprint. Discussion started: 3 November 2026
© Author(s) 2026. CC BY 4.0 License.

In the 2000–5000 m layer, the ORA spread is substantially larger (Fig. 2d), since there are some outliers among the ORA members. For instance, GLORYS2v4 shows a decreasing OHC trend (Fig. 2d), consistent with the Copernicus Marine Service product quality document, which reports persistent cooling in the deep temperature and heat content time series of GLORYS2v4 (Drévillon et al., 2023). However, the updated version, GLORYS4v2, has improved the representation of the OHC (Fig. 2d). GODAS shows an even stronger cooling trend below 2000 m, several times larger than that of GLORYS2v4 (Fig. 2d). However, aside from these outliers, the vast majority of ORAs show small rates of warming for this layer – rates as small as in the OAs. The global 2000–5000 m OHC trends are 0.095 W m^{-2} for IAPv4 and 0.067 W m^{-2} for ORA EM over 1993–2022 (Fig. 2d). For comparison, Johnson and Purkey (2024) estimated a global warming rate of 0.068 ± 0.016 W m^{-2} below 2000 m from 1987 to 2015.

https://doi.org/10.5194/egusphere-2026-6613
Preprint. Discussion started: 3 November 2026
© Author(s) 2026. CC BY 4.0 License.



285 **Figure 1. Global OHC anomalies from 1993 to 2024 for (a) 0–700 m, (b) 700–2000 m, (c) 0–2000 m, and (d) 2000–5000 m. Anomalies are referenced to 2005–2022. Colored shading indicates the 90% confidence interval (CI), as described in Section 2.2. OHC is expressed in zettajoules (ZJ, 1 ZJ = 10^{21} J).**

https://doi.org/10.5194/egusphere-2026-6613
Preprint. Discussion started: 3 November 2026
© Author(s) 2026. CC BY 4.0 License.

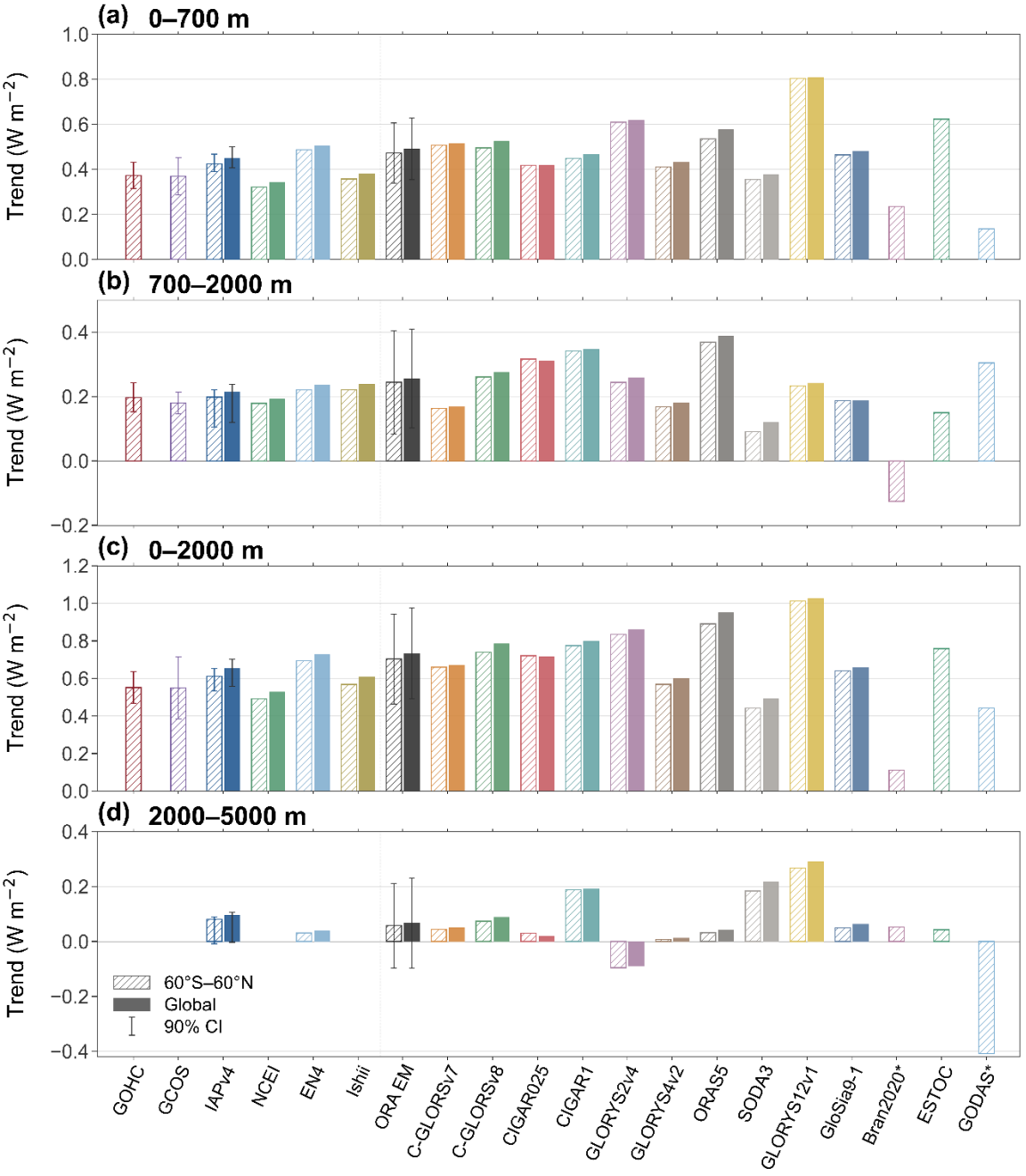


Figure 2. Global and 60°S–60°N OHC trends for (a) 0–700 m, (b) 700–2000 m, (c) 0–2000 m, and (d) 2000–5000 m. Trends are calculated over 1993–2022 for all products except GCOS and GloSia9-1, for which 1993–2020 are used because their data end in 2020. The Bran2020 and GODAS values in panel d represent trends of 2000-4509 m and 2000-4478 m, respectively, due to their limitation on maximum depth. Open symbols show OHC trends for 60°S–60°N, and filled symbols show global OHC trends. Error bars indicate the 90% CI.

https://doi.org/10.5194/egusphere-2026-6613
Preprint. Discussion started: 3 November 2026
© Author(s) 2026. CC BY 4.0 License.

3.2 Variability of Upper-2000 m OHC Tendencies and TOA Net Radiation

Satellite radiative flux measurements indicate an increase in Earth's energy imbalance (EEI) over the past two decades (Loeb et al., 2021). Following Trenberth et al. (2016), we compare monthly global upper-2000 m OHC tendencies from the ORA EM and three OA products with net top-of-atmosphere (TOA) radiation anomalies from CERES (Fig. 3). At the monthly scale, all OHC products exhibit substantially larger fluctuations than CERES (Fig. 3a). The standard deviations are 3.63 and 3.41 W m^{-2} for the ORA EM and IAPv4, respectively, much smaller than those of EN4 and Ishii, but still considerably larger than CERES (0.70 W m^{-2}). Following Trenberth et al. (2016), we apply a 1–2–1 smoothing filter, which uses weights of 0.25, 0.50, and 0.25 for three consecutive months, to reduce high-frequency fluctuations (Fig. 3b). We also calculate 12-month running means directly from the original monthly series (Fig. 3c). Both smoothing methods substantially reduce the fluctuations. After 12-month smoothing, the standard deviations decrease to 0.54 W m^{-2} for the ORA EM and 0.66 W m^{-2} for IAPv4, closer to CERES (0.41 W m^{-2}), while EN4 and Ishii retain considerably larger variability (Table 2). The temporal differencing amplifies high-frequency noise, which can contribute to the large month-to-month fluctuations in OHC tendencies (Trenberth et al., 2016).

The linear trends in the 12-month running mean OHC tendencies over January 2005–June 2023 are 0.29 [−0.21, 0.80] W m^{-2} $decade^{-1}$ for the ORA EM and 0.27 [0.10, 0.37] W m^{-2} $decade^{-1}$ for IAPv4, while EN4 and Ishii show smaller trends (Table 2). All four OHC products show smaller trends than CERES (0.54 W m^{-2} $decade^{-1}$). The inter-product uncertainty interval for the ORA EM spans zero, indicating that the magnitude and robustness of the increase in ocean heating rates remain strongly product-dependent. Nevertheless, the ORA EM provides the closest central trend estimate to CERES among the OHC products. In comparison, the IAPv4 ensemble shows a more robust positive trend, with its uncertainty range entirely above zero. Together with the variability analysis, these results suggest that the ORA EM and IAPv4 provide more consistent estimates of upper-ocean heating-rate variability with the CERES energy-budget constraint than EN4 and Ishii, although substantial uncertainties remain in the long-term trends.

https://doi.org/10.5194/egusphere-2026-6613
Preprint. Discussion started: 3 November 2026
© Author(s) 2026. CC BY 4.0 License.

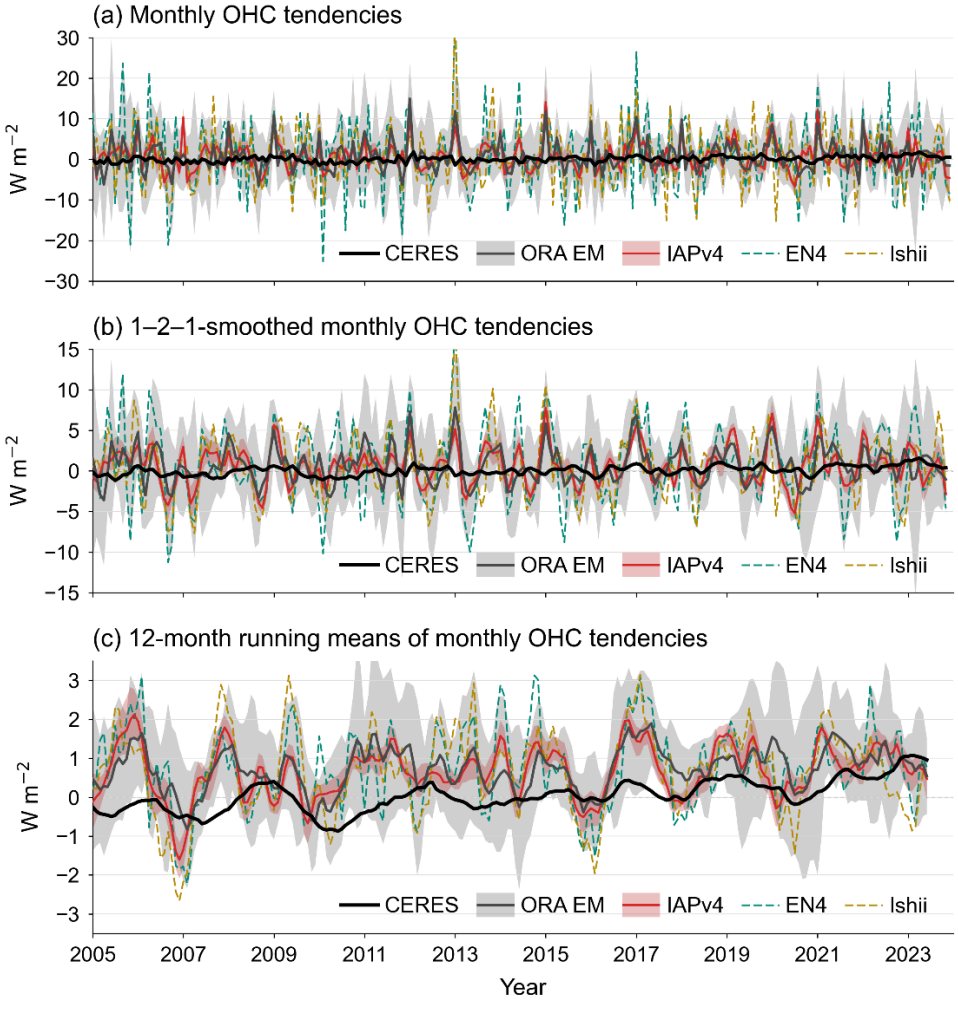


Figure 3. Monthly variability in upper-2000 m OHC tendencies and CERES net top-of-atmosphere (TOA) radiation from 2005 to 2023. OHC tendencies are calculated from differences between consecutive monthly OHC anomalies and expressed per unit Earth area (W m^{-2}). CERES shows anomalies of global net TOA radiation. The OHC products are IAPv4, EN4, Ishii, and the eight-reanalysis ensemble mean (ORA EM). (a) Monthly series; (b) the same series after 1–2–1 smoothing; (c) centered 12-month running means calculated directly from the series in panel (a). Each product's 2005–2022 monthly climatology was removed. Red shading shows the 5th–95th percentile range of 918 IAPv4 members; gray shading shows ORA EM ±1.65 times the standard deviation across its eight members. Complete smoothing windows end in November 2023 in (b) and June 2023 in panel (c).

https://doi.org/10.5194/egusphere-2026-6613
Preprint. Discussion started: 3 November 2026
© Author(s) 2026. CC BY 4.0 License.

Table 2. For each of the given global OHC products and CERES, included are the following: autocorrelation (AC) at lag-1 month of OHC (or CERES equivalent); the monthly standard deviation (std dev) of the monthly rates of change of OHC (W m^{-2}); the corresponding standard deviation if smoothed with a 0.25 (1–2–1) smoother; standard deviation of the 12-month running mean; and the linear trend of the 12-month running mean (W m^{-2} decade^{-1}). Brackets indicate the 90% uncertainty ranges for ORA EM and IAPv4. All values are for 2005–2023 and 0–2000 m depth.

Product	Lag-1 AC	Std dev	Std dev (1-2-1)	Std dev (12 month)	Trend (W m^{-2} decade^{-1})
ORA EM	0.997	3.629	2.177	0.542	0.293 [−0.212, 0.799]
IAPv4	0.997	3.412	2.282	0.662	0.256 [0.100, 0.370]
EN4	0.983	8.969	4.687	1.006	0.171
Ishii	0.988	7.182	3.769	1.078	0.183
CERES	0.999	0.703	0.563	0.407	0.542

3.3 Spatial trend patterns and regional product dependence

Both OAs and the ORA EM show widespread warming in 0–2000 m OHC during 1993–2022, and their large-scale spatial patterns are broadly consistent (Fig. 4 and Fig. 5). These products show a strong warming trend in the Atlantic basin, with the exception of the cooling trend in the Subpolar gyre (i.e. "North Atlantic Warming Hole"). The products show a pronounced and robust warming in the North Pacific, consistent with the northward displacement of the Kuroshio. There is also substantial warming in the Indian Ocean and Western Pacific, and most of the Southern Ocean. The only areas where both OAs and ORAs show a cooling trend are in the above mentioned North Atlantic Warming Hole, the Eastern Equatorial Pacific and the Southern Ocean by the equatorward edges of the sub-Antarctic Front and Polar Front.

However, the difference between the OAs and ORA EM shows regional structure. For example, large differences between OAs (IAPv4 and EN4) and ORA EM occur mainly in regions with strong meso-scale dynamics and large-scale gradients, including the North Atlantic western boundary current (WBC) and its extension, the Kuroshio Extension, the Antarctic Circumpolar Current (ACC) and its frontal systems and the Agulhas Return Current region (Fig. 4b and c). A notable large-scale difference between the ORA EM and the individual OAs (Fig. 4b and c; Fig. S3) is evident in the tropical Pacific, characterized by a

https://doi.org/10.5194/egusphere-2026-6613
Preprint. Discussion started: 3 November 2026
© Author(s) 2026. CC BY 4.0 License.

dipole pattern: the ORA EM shows a stronger warming trend in the western Pacific and a weaker warming trend in the eastern Pacific (Fig. 4b and c). Overall, the global mean absolute difference (MAD) of IAPv4 and the ORA EM in OHC trend is slightly lower than that of EN4 (Fig. 4b and c). EN4-derived trends should be interpreted with caution in areas with low observation weights, where the analyses are more strongly influenced by background fields (Killick, 2021).

Significant differences among ORAs are also found in regions with strong meso-scale activity (Fig. 4d), where OHC changes are highly sensitive to the position of current axes, frontal slopes, and eddy activity. This means that a small displacement relative to the grid scale can produce large OHC differences among products. The similar features are also present among the OAs, but with a smaller magnitude (Fig. 4e). Inter-product differences among ORAs are smaller in the subtropical gyres, the tropical Indian Ocean, and parts of the tropical Pacific (Fig. 4d).

https://doi.org/10.5194/egusphere-2026-6613
Preprint. Discussion started: 3 November 2026
© Author(s) 2026. CC BY 4.0 License.

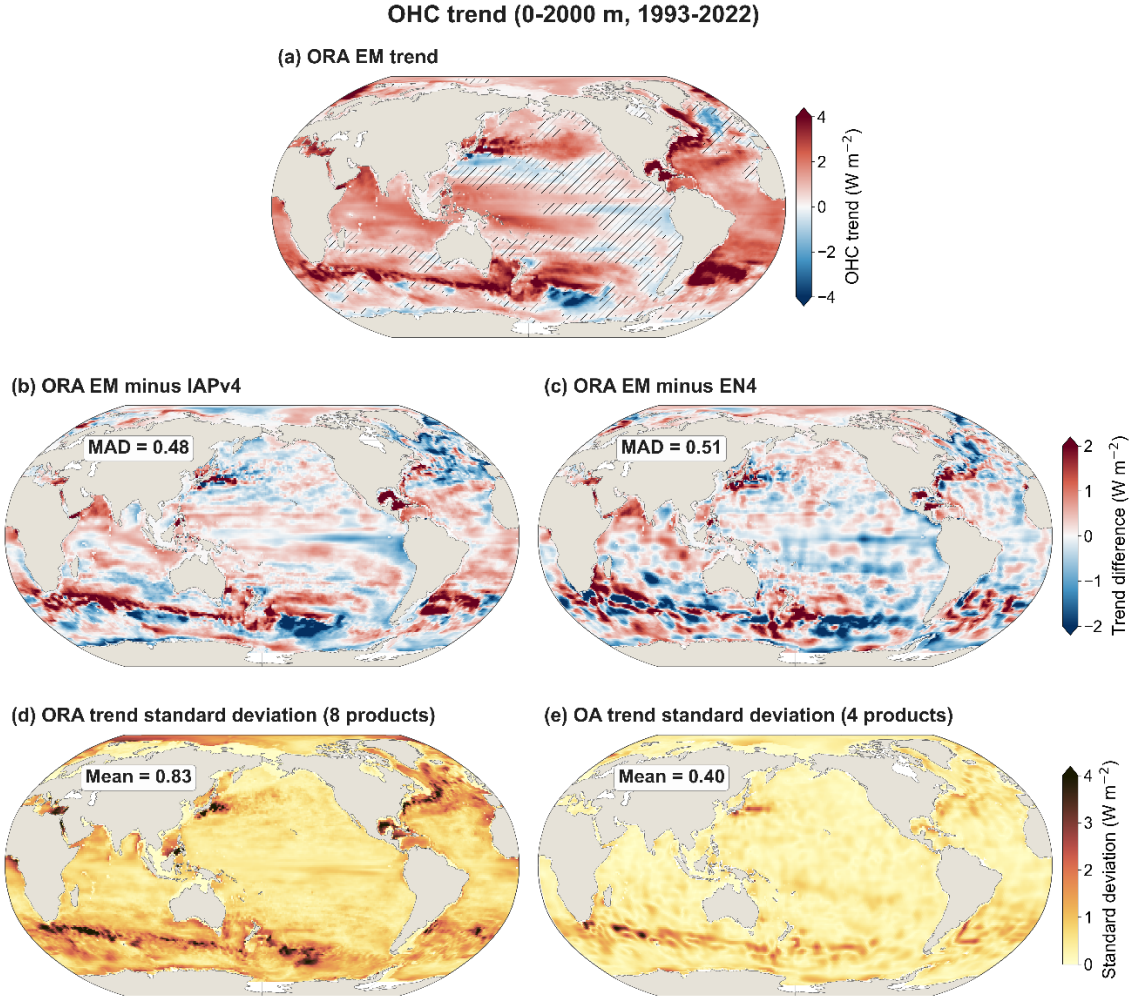


Figure 4. Spatial patterns of 0–2000 m OHC trends and product spread during 1993–2022. Panel (a) shows the eight-product ORA EM trend. Panels (b, c) show ORA EM minus IAPv4 and EN4, respectively. Panels (d, e) show the standard deviation of OHC trends across eight ORAs and four OAs, respectively. Hatching in panel (a) marks grid cells where the linear trend is not statistically significant at the 90% confidence level. Boxed mean absolute difference (MAD) values are global ocean area-weighted mean absolute differences. Boxed Mean values are area-weighted means of the displayed standard-deviation fields. All mapped quantities and boxed statistics are expressed in W m^{-2}.

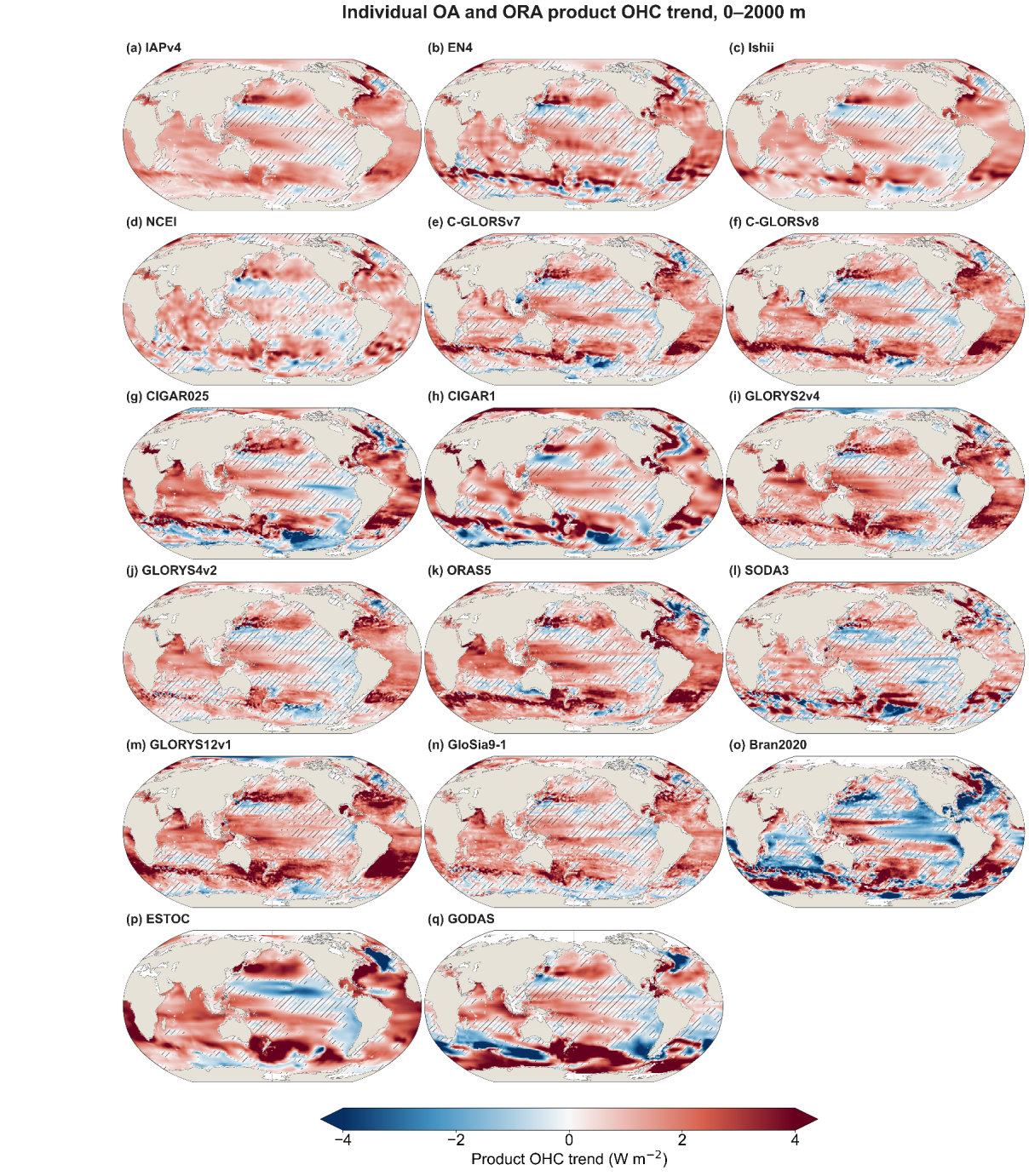
Figure 5 shows the 0–2000 m OHC trends in individual OAs and ORAs. The four OAs exhibit broadly similar and relatively smooth large-scale patterns (Fig. 5a-d), likely reflecting their reliance on largely the same in situ data, statistical mapping, objective analysis, and spatial smoothing. Compared with the other

https://doi.org/10.5194/egusphere-2026-6613
Preprint. Discussion started: 3 November 2026
© Author(s) 2026. CC BY 4.0 License.

OAs, EN4 shows stronger OHC trends in western boundary currents and the ACC regions (Fig. 5a-d). Consistent with the spatial pattern of the warming trend in OAs, most ORAs show warming in the Atlantic Ocean, many high-latitude regions of the Northern Hemisphere, and parts of the Southern Ocean. However, substantial differences remain in WBC, ACC and high-latitude regions. For example, most products show Arctic warming, whereas GLORYS2v4 and GLORYS12v1 show cooling in parts of the Arctic Ocean (Fig. 5i and m). Among all the ORAs, BRAN2020 shows a cooling trend in the North WBC region and also broad cooling in the Pacific and Indian Oceans, which may be caused by its relatively high early-period OHC anomalies shown in Fig. S1. These individual-product maps show that the regional trend structure can differ substantially even when the basin-scale warming signal is broadly consistent across products. Most products show a relatively small trend below 2000 m (Fig. S4).

These ORAs span a wide range of horizontal resolutions, from coarse non-eddy-resolving grids (1°) to eddy-permitting (1/4°) and nominally eddy-resolving (1/12°) configurations (Table 1). In dynamically active regions, coarse-resolution models cannot explicitly resolve mesoscale eddies. They therefore rely more strongly on eddy parameterizations and are also subject to stronger numerical smoothing, which tends to smooth sharp local warming or cooling signals. This is evident, for example, in ESTOC, CIGAR1 and GODAS, which show relatively smooth OHC changes in western boundary current regions (Fig. 5h, p and q). In contrast, GLORYS and C-GLORS products for example, with horizontal resolution higher than 1°, can retain sharper local frontal gradients in dynamically active regions, even after remapping to the common 1° grid (e.g. Fig. 5m). This difference between resolving and parameterizing mesoscale processes can lead to substantial product-dependent differences in the horizontal and vertical redistribution of heat in these regions (Chassignet and Xu, 2017).

https://doi.org/10.5194/egusphere-2026-6613
Preprint. Discussion started: 3 November 2026
© Author(s) 2026. CC BY 4.0 License.



395 **Figure 5. Individual OA and ORA trends in 0–2000 m OHC. Panels (a–d) show the four OAs, and panels (e–q) show the individual ORAs. Trends are calculated over 1993–2022, except for GloSia9-1, for which 1993–2020 is used because its data end in 2020. Hatching marks grid cells where the linear trend is not statistically significant at the 90% confidence level.**

https://doi.org/10.5194/egusphere-2026-6613
Preprint. Discussion started: 3 November 2026
© Author(s) 2026. CC BY 4.0 License.

3.4 Latitude-depth structure of OHC trends

The latitude-depth diagnostics show where, and at which depths, the seawater temperature trend is consistently represented among products and where it remains most product dependent (Fig. 6 and 7). During 1993–2022, both the OAs and the ORA EM are dominated by positive temperature trends, particularly in the upper 2000 m (Fig. 6 and 7). Both the OAs and the ORA EM show the strongest upper-2000-m warming in the mid-latitudes, followed by the high latitudes of the Northern Hemisphere, where the warming extends to greater depths than the Southern Hemisphere (Fig. 6a and 7a–d).

The differences between the ORA EM and individual OAs vary among datasets (Fig 6b and c). Compared with IAPv4, the ORA EM shows stronger warming between the equator and 45°S, but weaker warming near the surface of the Southern Ocean (Fig. 6b). Compared with EN4, the ORA EM shows weaker upper-ocean warming across most of the Southern Hemisphere, whereas stronger warming occurs at some latitudes and depths in the Northern Hemisphere (Fig. 6c). Pronounced differences between the OAs and the ORA EM are also found in the 2000–5000 m layer of the Southern Hemisphere middle-to-high latitudes and in the deep Arctic Ocean (Fig. 6b and c). The latitude–depth difference patterns between the ORA EM and Ishii or NCEI in the upper 2000 m are broadly similar to those between the ORA EM and IAPv4 (Fig. S5).

The Arctic shows the largest ORA spread, especially in the deep ocean north of 80°N (Fig. 6d). This may mainly be caused by the fact that Arctic observations are much sparser than North Atlantic observations and that reanalyses products differ in their representation of deep-water formation and ocean heat transport from Atlantic warm water. In this region, seawater temperature estimates are sensitive to sea ice–ocean coupling, open-water fraction, stratification, vertical mixing, and the representation of Atlantic inflow. The near-Antarctic Southern Ocean also shows large ORA spread from the upper ocean to about 2000 m (Fig. 6d). In the Southern Ocean, surface heat uptake can be redistributed away from the Antarctic margin and into the ocean interior by the overturning circulation, including circumpolar upwelling and northward transport (Armour et al., 2016). As a result, seawater temperature trends near the Antarctic are spatially heterogeneous and can be represented differently among ORAs. However, there is a subtle but consistent warming of bottom waters in the deep Southern Ocean around 4000 m near 60°S (Fig. 6a).

https://doi.org/10.5194/egusphere-2026-6613
Preprint. Discussion started: 3 November 2026
© Author(s) 2026. CC BY 4.0 License.

Figure 7 shows the latitude-depth structure of seawater temperature trends in individual OAs and ORAs. Most products show positive trends in the upper ocean, and the OAs exhibit broadly similar large-scale patterns within their common depth ranges. In contrast, the ORAs show substantial differences. These differences are especially pronounced below 2000 m. Most ORAs show weak deep-ocean warming, whereas some products show strong deep cooling or localized deep warming. For example, BRAN2020 and GODAS show large cooling below 2000 m in the low- and mid-latitude oceans (Fig. 7o and q); SODA3 and GODAS show large deep warming in the Southern Ocean, with the signal extending toward lower latitudes in the deep ocean (Fig. 7l and q). Between these end members, clear differences also occur among products from the same family or similar systems. GLORYS2v4, GLORYS4v2 and GLORYS12v1 exhibit marked differences in the deep layer (Fig. 7i, j and m); and CIGAR1 and CIGAR025 differ substantially at high latitudes and in the deep ocean (Fig. 7g and h). These results indicate that the vertical structure of OHC trends can be sensitive to model physics, resolution, assimilation methods, and the types of observational variables assimilated, particularly in data-sparse regions. Therefore, products from the same centre or product family should not be treated as equivalent when evaluating regional or depth-dependent seawater temperature changes.

https://doi.org/10.5194/egusphere-2026-6613
Preprint. Discussion started: 3 November 2026
© Author(s) 2026. CC BY 4.0 License.

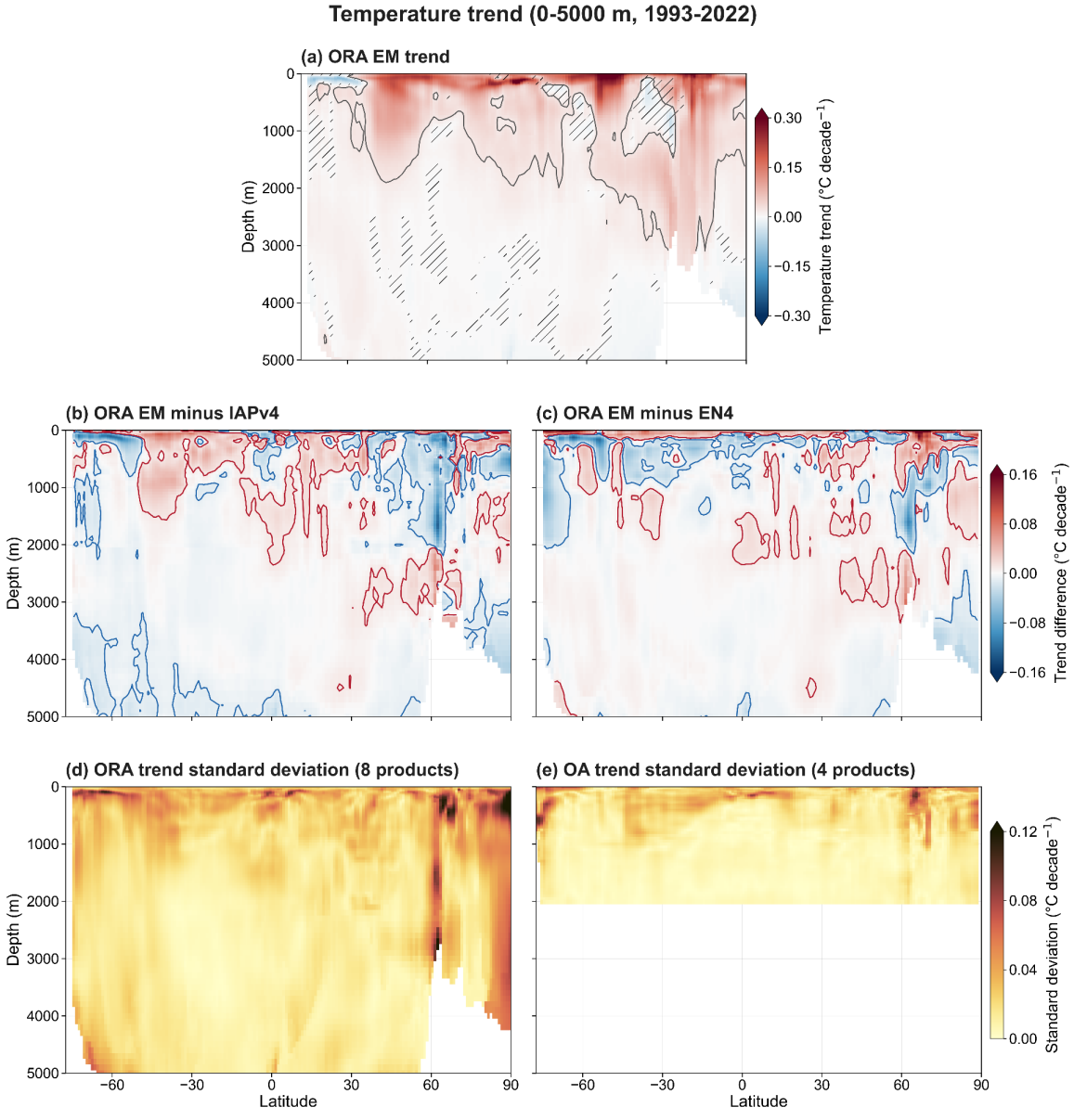


Figure 6. Latitude–depth structure of zonal-mean temperature trends during 1993–2022. Panel (a) shows the eight-product ORA EM trend. Panels (b, c) show ORA EM minus IAPv4 and EN4, respectively. Panels (d, e) show the standard deviation of temperature trends across eight ORAs and four OAs, respectively. Hatching in panel (a) marks locations where the linear trend is not statistically significant at the 90% confidence level. The grey contour in panel (a) marks +0.02 °C decade^{-1}, and blue and red contours in panels (b, c) mark −0.01 and +0.01 °C decade^{-1}, respectively. Panel (e) is blank below 2000 m because Ishii and NCEI are unavailable below 2000 m.

https://doi.org/10.5194/egusphere-2026-6613
Preprint. Discussion started: 3 November 2026
© Author(s) 2026. CC BY 4.0 License.

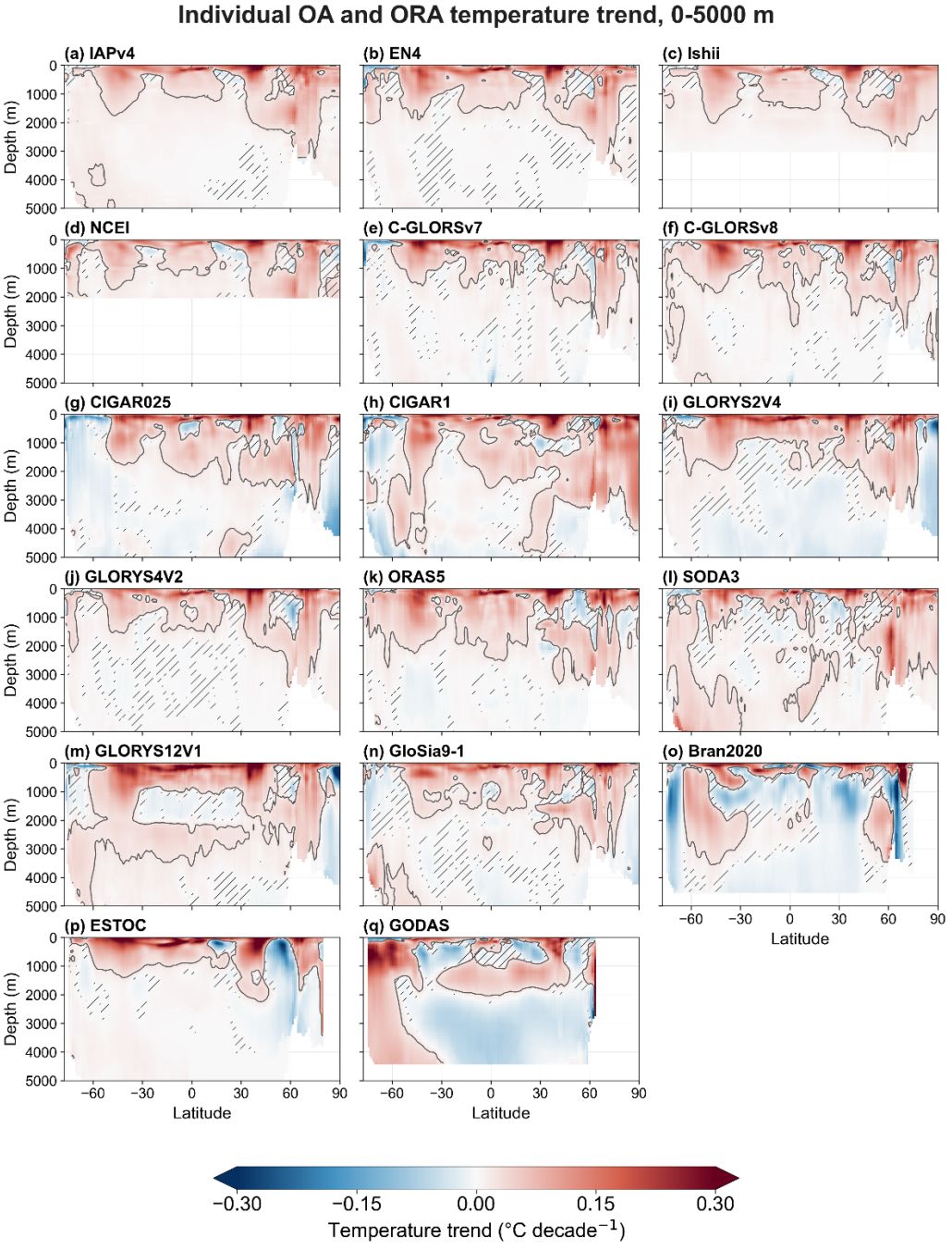


Figure 7. Latitude–depth temperature trends in individual OAs and ORAs. Panels (a–d) show the four OAs, and panels (e–q) show the individual ORAs. Trends are calculated over 1993–2022, except for GloSia9-1, for which 1993–2020 is used because its data end in 2020. Grey contours mark +0.02 °C decade^{-1}. Hatching marks locations where the linear trend is not statistically significant at the 90% confidence level.

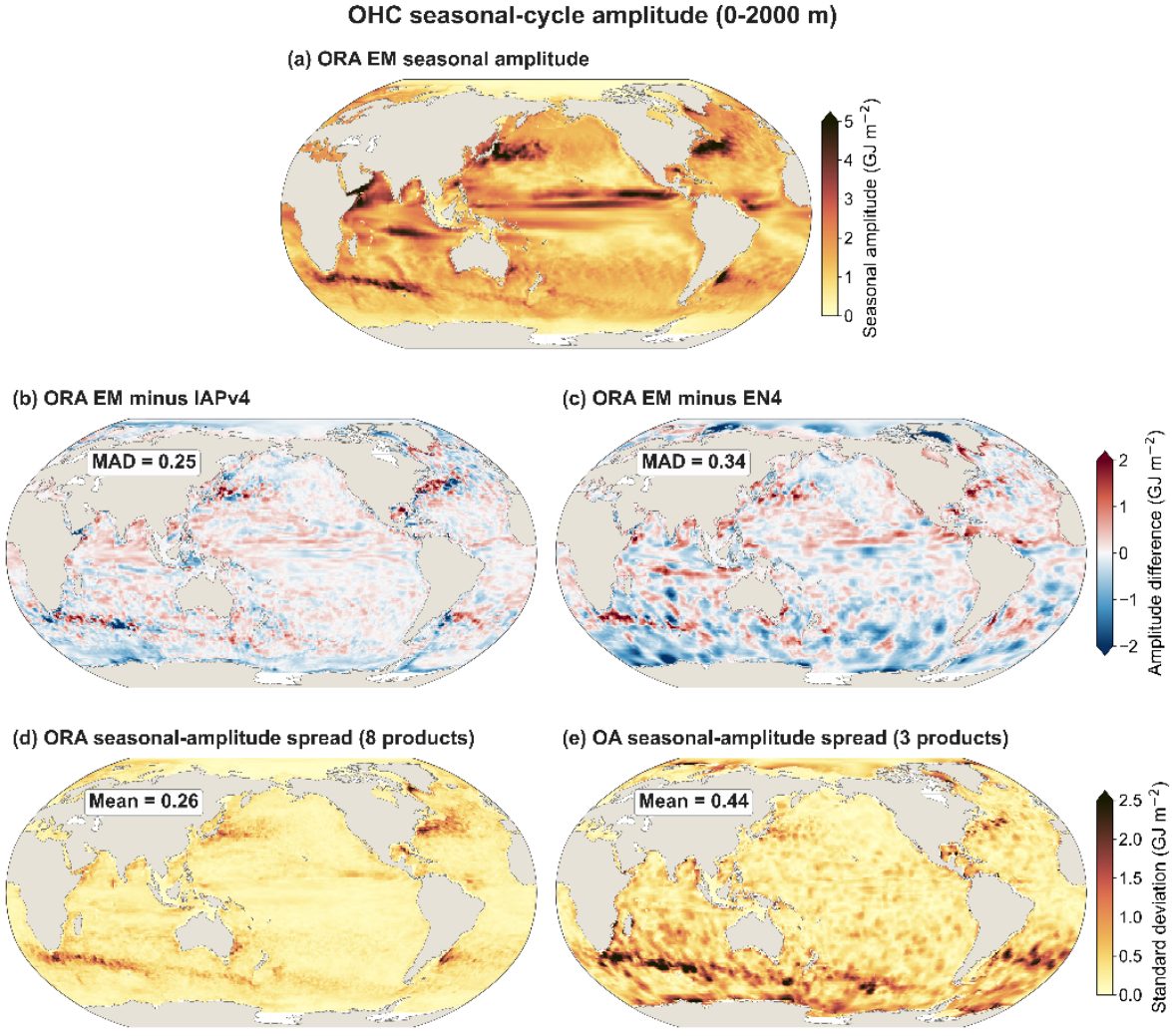
https://doi.org/10.5194/egusphere-2026-6613
Preprint. Discussion started: 3 November 2026
© Author(s) 2026. CC BY 4.0 License.

3.5 Seasonal amplitude

The annual cycle of OHC describes the strength of regular heat storage and heat release by the ocean within a year (Forget, 2010; Palmer et al., 2017). Unlike the long-term OHC increase, which mainly reflects net ocean heat uptake, the seasonal-cycle amplitude is more directly affected by seasonal radiation, air–sea heat fluxes, mixed-layer depth, wind-driven transport, and local circulation (Johnson et al., 2024; Pan et al., 2023). It therefore provides an additional diagnostic for assessing whether ORA and OAs show consistent seasonal heat-storage structures. In this study, the seasonal amplitude at each grid point is defined as the difference between the maximum and minimum values of the 12-month climatology (1993–2022) after removing the long-term trend.

In the 0–2000 m layer, individual OAs and ORAs show similar high-amplitude bands (Fig. S6). The ORA EM shows a clear narrow east–west band that appears in the equatorial Pacific. Strong seasonal amplitudes are also found in the Kuroshio Extension in the North Pacific, the Gulf Stream and its extension in the North Atlantic, the southern Indian Ocean–Agulhas system, the Southern Ocean frontal zone, and several WBC and basin-boundary regions (Fig. 8a). Pan et al., (2023) showed that eddy-induced advection can make an important contribution to the annual cycle of OHC in regions with high eddy kinetic energy, such as WBC and ACC. Compared with IAPv4 and EN4, ORA EM exhibits stronger seasonal amplitude in the WBC and ACC regions, while it is weaker in polar regions (Fig. 8b and c). The global MAD of IAPv4 and the ORA EM in seasonal amplitude are lower than that of EN4 (Fig. 8b and c). The inter-product spread in seasonal amplitude is larger among the OAs than among the ORAs (Fig. 8d and e), mainly because Ishii shows a substantially larger seasonal amplitude than IAPv4 and EN4 (Fig. S6).

https://doi.org/10.5194/egusphere-2026-6613
Preprint. Discussion started: 3 November 2026
© Author(s) 2026. CC BY 4.0 License.



475 **Figure 8. Seasonal-cycle amplitude of 0–2000 m OHC. Seasonal amplitude is defined as the maximum-minus-minimum range of the detrended 12-month climatology (1993-2022). Panel (a) shows the eight-product ORA EM. Panels (b, c) show ORA EM minus IAPv4 and EN4, respectively. Panels (d, e) show the standard deviation across eight ORA and three OAs, respectively. Boxed MAD values in panels (b, c) are global ocean area-weighted mean absolute differences. Boxed Mean values in panels (d, e) are area-weighted means of the displayed standard-deviation fields. The OA spread**
480 **includes IAPv4, EN4 and Ishii; NCEI is excluded because no monthly field is available before 2005.**

https://doi.org/10.5194/egusphere-2026-6613
Preprint. Discussion started: 3 November 2026
© Author(s) 2026. CC BY 4.0 License.

3.6 Inter-product agreement in OHC interannual variability and trend

The S/N directly indicates whether the common interannual variability or trend in OHC represented by the ORA EM is stronger than the spread among individual products. For interannual variability, regions with S/N > 1 before 2005 were mainly located in the upper ocean of the low- to mid-latitude Pacific and parts of the Indian Ocean (Fig. 9a, b). These regions largely coincide with areas strongly influenced by major modes of interannual climate variability, including the El Niño–Southern Oscillation and the Indian Ocean Dipole. For the OHC trend, regions with S/N > 1 before 2005 were mainly located in the western Pacific, North Pacific, and subpolar North Atlantic (Fig. 10a, b).

After 2005, the area with S/N > 1 expanded substantially in the upper 2000 m for both interannual variability and trends. For interannual variability, the fraction of the ocean area with S/N > 1 increased from 52.9% during 1993–2004 to 73.7% during 2005–2022 (Fig. 9g, h), with much of the increase occurring in the Southern Ocean, northern Indian Ocean, and Atlantic Ocean. Both the 0–700 m and 700–2000 m layers contributed to this increase (Fig. 9c, f), with the largest increase occurring at 700–2000 m. In contrast, the fraction of the ocean area with S/N > 1 at 2000–5000 m showed little change between the two periods (Fig. 9j–l). For the OHC trend, the fraction of the ocean area with S/N > 1 in the upper 2000 m increased from 44.2% during 1993–2004 to 65.5% during 2005–2022 (Fig. 10g, h). The increase was widespread across the Atlantic Ocean, the mid-latitude Pacific, and the Indian Ocean. However, in some regions of the low-latitude Pacific and southern Indian Ocean, S/N decreased from values above 1 to below 1 (Fig. 10i). Similar to the results for interannual variability, the largest increase occurred in the 700–2000 m layer (Fig. 10f). These improvements for the inter-product agreement are consistent with the strengthened observational constraints in the upper 2000 m during the Argo era.

To assess whether the different lengths of the two comparison periods affected these results, we additionally calculated both S/N metrics for seven 12-year moving windows from 2005–2016 through 2011–2022 and compared each of them with the 1993–2004 period (Fig. S7 and S8). The main results remained consistent across these equal-length comparisons, indicating that the difference in window length does not materially affect our main conclusions. The OAs also show a clear increase after 2005 in the area with S/N > 1 for both interannual variability and OHC trend, although the increase is smaller

https://doi.org/10.5194/egusphere-2026-6613
Preprint. Discussion started: 3 November 2026
© Author(s) 2026. CC BY 4.0 License.

than that for the ORA (Fig. S9 and S10). This smaller increase reflects the already extensive areas with S/N > 1 in the OAs before 2005. During 2005–2022, the fractions of the ocean area with S/N > 1 reached 95.5% for interannual variability and 84.6% for trends (Fig. S9h and S10h, respectively).

Taylor diagrams provide a complementary view of product agreement by evaluating whether different products reproduce similar OHC anomaly structures (Fig. 11). In the 0–700 m layer, product points are closely clustered. Most products show high correlations with the ORA EM, and their normalized standard deviations are close to 1 (Fig. 11a). This indicates that upper-ocean OHC anomalies contain a clear common spatiotemporal signal across products. Agreement weakens with depth. In the 700–2000 m layer, the distances between individual products and the ORA EM become larger (Fig. 11b). The largest product differences occur in the 2000-5000 m layer, where many products have lower correlations and normalized standard deviations that strongly deviate from 1 (Fig. 11d). Some ORAs show deep-ocean anomaly amplitudes several times larger than those of the ORA EM. Taylor diagrams for 60°S–60°N show conclusions that are generally consistent with the global results (Fig. S11).

https://doi.org/10.5194/egusphere-2026-6613
Preprint. Discussion started: 3 November 2026
© Author(s) 2026. CC BY 4.0 License.

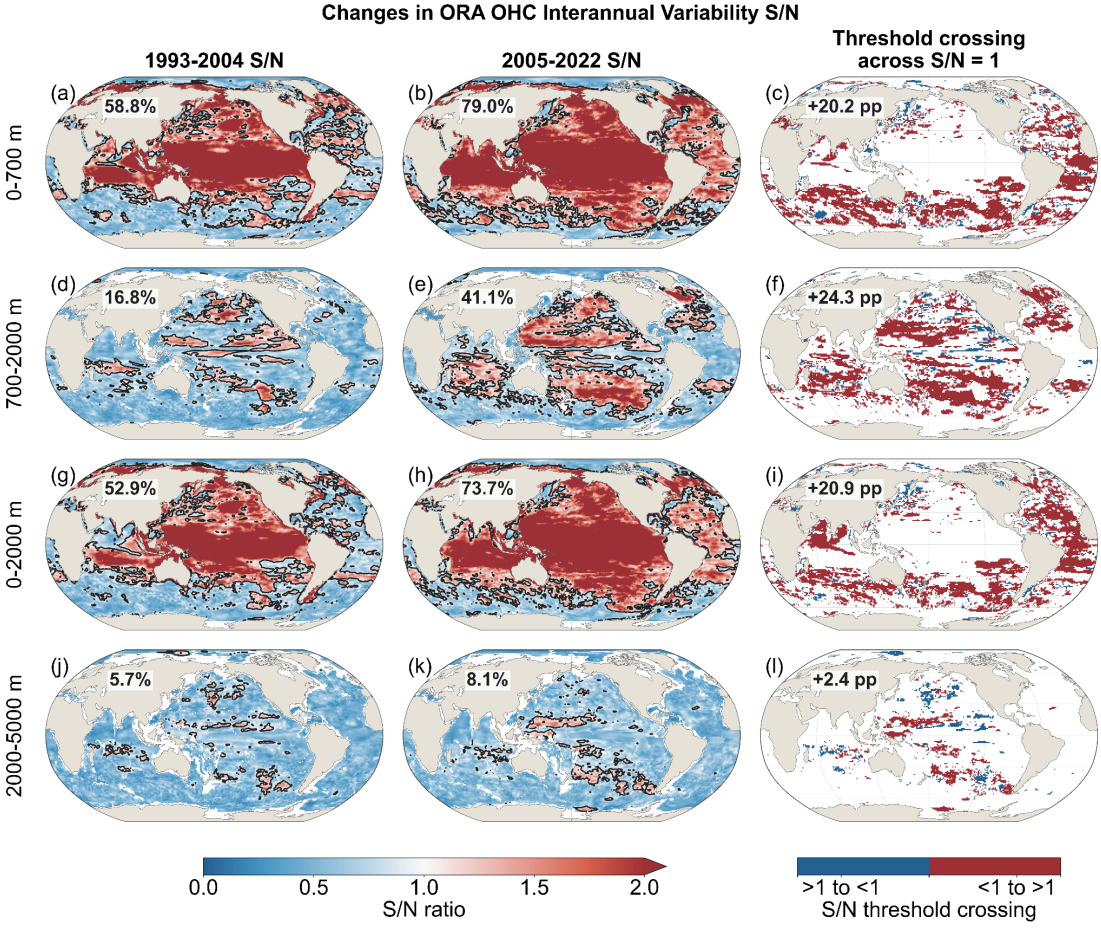


Figure 9. Changes in the ORA OHC interannual signal-to-noise ratio (S/N) across the Argo transition. Rows show 0–700 m, 700–2000 m, 0–2000 m, and 2000–5000 m, respectively. The first two columns show S/N for 1993–2004 and 2005–2022, respectively, and the third column shows crossings of the S/N = 1 threshold. Black contours mark S/N = 1. Percentage labels in the first two columns indicate the valid ocean area with S/N > 1. In the third column, percentage labels indicate changes in the ocean-area fraction with S/N > 1 in percentage points (pp).

https://doi.org/10.5194/egusphere-2026-6613
Preprint. Discussion started: 3 November 2026
© Author(s) 2026. CC BY 4.0 License.

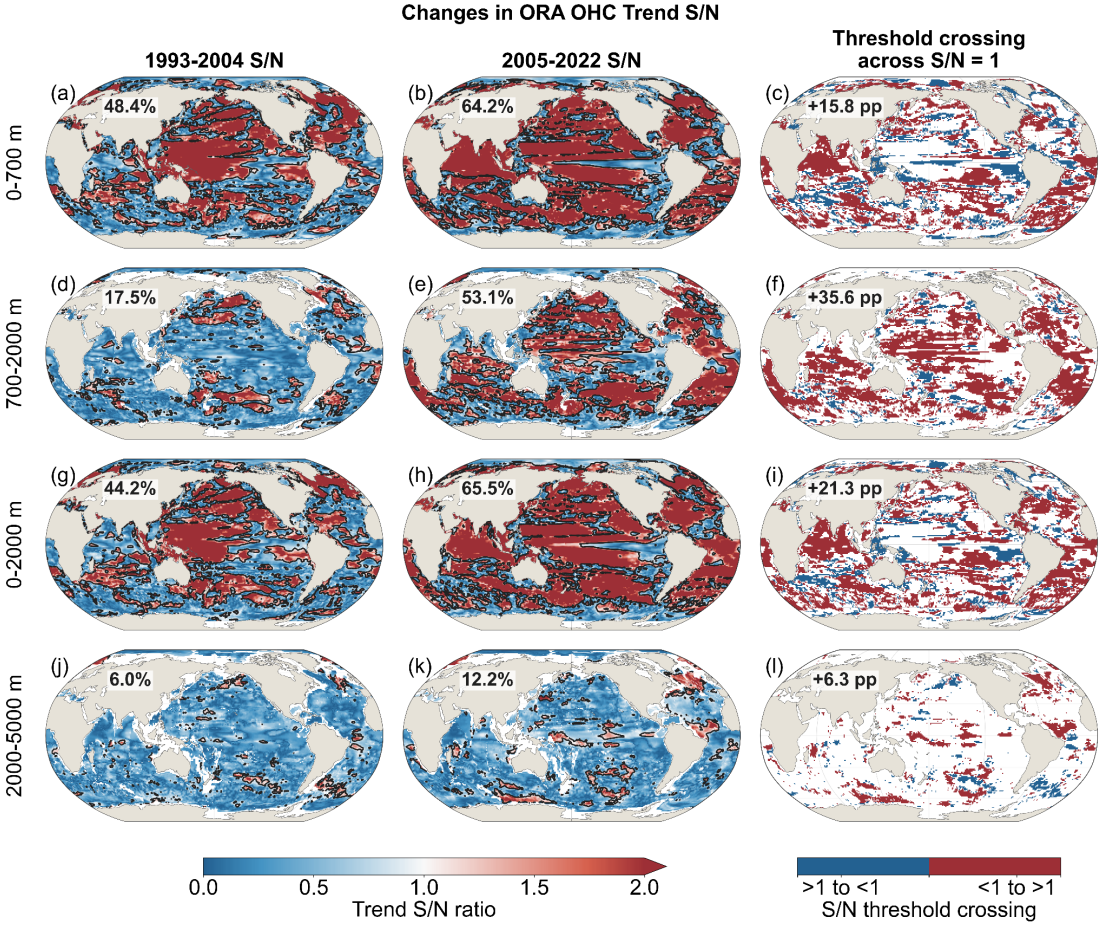
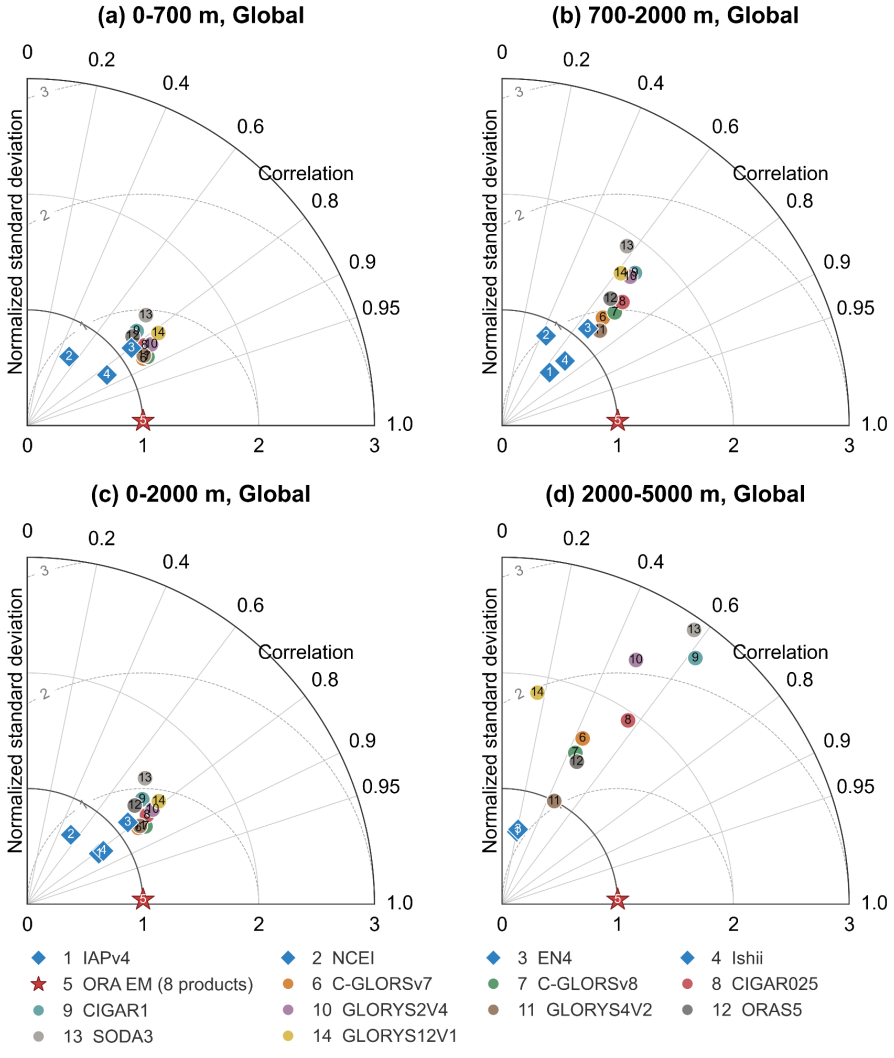


Figure 10. Same as Figure 9, but for ORA OHC trend S/N.

https://doi.org/10.5194/egusphere-2026-6613
Preprint. Discussion started: 3 November 2026
© Author(s) 2026. CC BY 4.0 License.



530 **Figure 11. Taylor-diagram comparison of global OHC anomalies against the ORA EM. Panels (a–d) show 0–700 m, 700–2000 m, 0–2000 m, and 2000–5000 m, respectively. Metrics are calculated from annual OHC anomalies over 1993–2023 relative to each product's 2005–2022 mean. Angular position indicates the correlation with the ORA EM, radial distance indicates the standard deviation normalized by that of the ORA EM, and grey dashed arcs indicate the normalized centered root-mean-square difference. The red star marks the ORA EM, blue diamonds denote OAs, and**
535 **circles denote individual ORAs.**

https://doi.org/10.5194/egusphere-2026-6613
Preprint. Discussion started: 3 November 2026
© Author(s) 2026. CC BY 4.0 License.

3.7 Comparison with ORA-IP reanalyses

This section compares the consistency of OHC estimates from the ORA ensemble used in MER-EP with those from ORA-IP (Palmer et al., 2017). The comparison focuses on the spatial distribution of S/N and the ensemble spread of the corresponding OHC time series. To avoid the influence of different ensemble sizes on the S/N calculation, we calculated the S/N and ensemble spread for all 495 possible 8-member combinations drawn from the 12 ORA-IP products.

For both OHC interannual variability and trend, the ORA ensemble used in MER-EP shows higher internal consistency than all ORA-IP combinations. In the upper 1500 m, the fraction of ocean area with S/N > 1 for interannual variability is 59.87% for the MER-EP ORA ensemble, compared with a mean of 48.61% and a maximum of 57.91% across the ORA-IP combinations (Fig. 12e). For the OHC trend, the corresponding fraction is 54.93% for the MER-EP ORA ensemble, whereas the mean and maximum values across the ORA-IP combinations are only 31.24% and 39.66%, respectively (Fig. 12f). Thus, none of the ORA-IP combinations reaches the level of internal consistency found in the MER-EP ORA ensemble. The improvement is particularly pronounced for OHC trends, indicating substantially greater agreement among the newer-generation reanalyses in their representation of OHC trends. This result provides further evidence of improvements in the newer-generation reanalyses systems and increases confidence in the use of ORAs for assessing OHC changes.

We further compared the OHC time series and ensemble spread between the ORA ensemble used in this study and the ORA-IP combinations (Fig. 13). In the upper 1500 m during 1993–2010, the mean ensemble spread is 40.3 ZJ for the MER-EP ORA ensemble, compared with a median of 60.6 ZJ across the ORA-IP combinations. Even the ORA-IP combination with the smallest spread has a value of 41.9 ZJ, which remains larger than that of the MER-EP ORA ensemble (Fig. 13). Figure 13 also shows a more pronounced adjustment in the MER-EP ORA ensemble during the transition to the Argo era. Overall, these comparisons indicate that the ORA ensemble used in MER-EP exhibits greater consistency in upper-ocean OHC than the ORA-IP combinations, while also showing a stronger common adjustment around 2005.

https://doi.org/10.5194/egusphere-2026-6613
Preprint. Discussion started: 3 November 2026
© Author(s) 2026. CC BY 4.0 License.

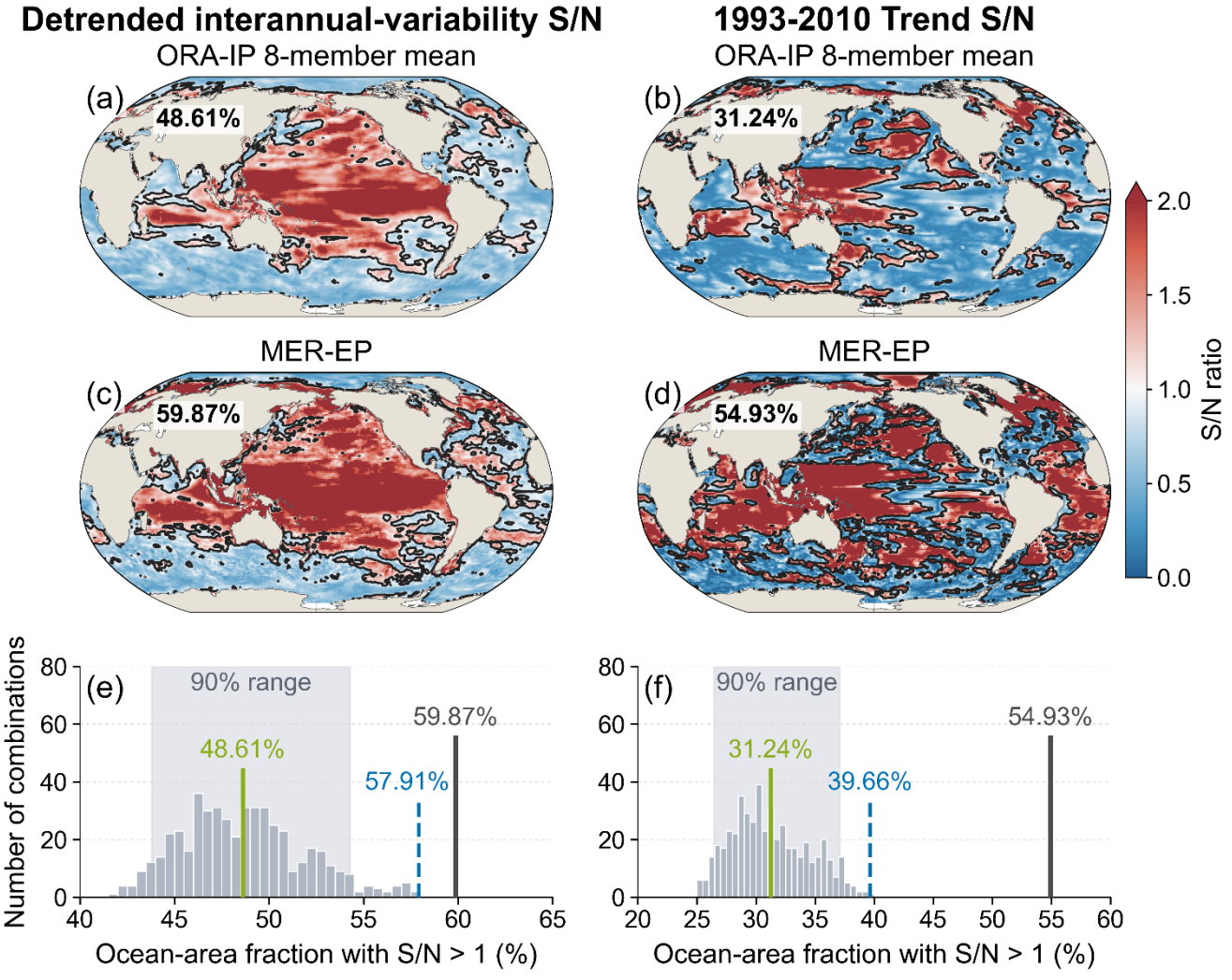


Figure 12. Comparison of 0–1500 m OHC S/N between ORA-IP and MER-EP (the eight ORAs used in this study) during 1993–2010. Panels (a, c and e) show results for detrended interannual variability, and panels (b, d and f) show results for linear trends. Panels (a, b) show the mean S/N across all 495 eight-member combinations drawn from the 12 ORA-IP products, and panels (c, d) show the fixed eight-member MER-EP ensemble. Black contours mark S/N = 1, and percentage labels indicate the valid ocean area with S/N > 1. Panels (e, f) show the distributions of the ocean-area fraction with S/N > 1 across the 495 ORA-IP combinations. Grey shading indicates the central 90% range, while the solid green, dashed blue, and solid dark-grey lines indicate the ORA-IP combination mean, ORA-IP maximum, and MER-EP value, respectively.

https://doi.org/10.5194/egusphere-2026-6613
Preprint. Discussion started: 3 November 2026
© Author(s) 2026. CC BY 4.0 License.

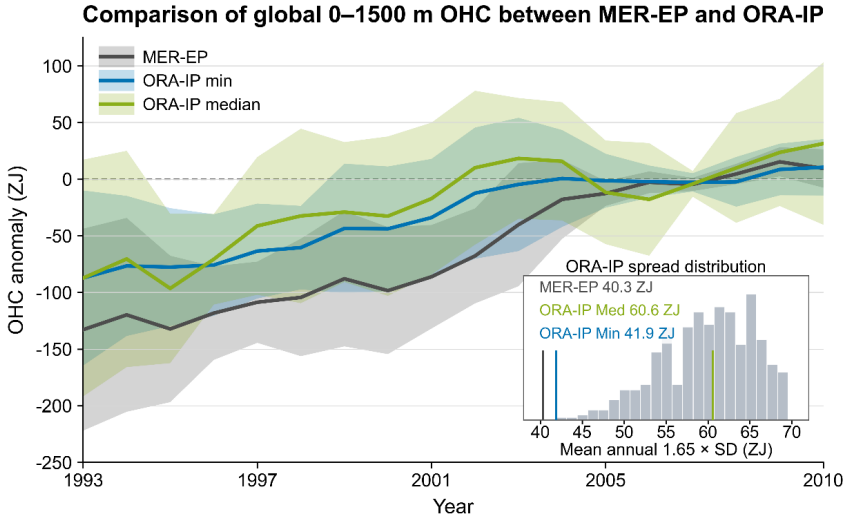


Figure 13. Global 0–1500 m OHC anomalies and inter-product spread in MER-EP and ORA-IP during 1993–2010. Annual anomalies are referenced to each member's 2005–2010 mean. The grey line shows the MER-EP ensemble mean, and the blue and green lines show the ORA-IP combinations with the minimum and median 1993–2010 mean spread, respectively. Shading indicates 90% CI. The inset histogram shows the distribution of the 1993–2010 mean spread across all 495 eight-member ORA-IP combinations. Grey, blue, and green vertical lines indicate the MER-EP ensemble, minimum-spread ORA-IP combination, and median-spread ORA-IP combination, respectively.

4 Discussion

The multi-product comparison shows that recent-generation ORAs and observation-based OAs provide a broadly consistent representation of large-scale OHC changes since 1993, including the long-term increase in OHC and its major spatial and vertical structures. More importantly, the recent-generation ORAs show substantially improved inter-product consistency, both across the transition into the Argo era and relative to the earlier-generation ORA-IP products, which strengthens confidence in the use of multi-reanalysis estimates for assessing large-scale OHC variability and trends. Large uncertainties remain in poorly observed regions and in the deep ocean, both in the ORAs and OAs.

In recent years, progress has been made in improving model resolution, surface forcing, bias correction, sea ice–ocean coupling, and data assimilation methods (e.g., Chamberlain et al., 2021; Forget et al., 2015; Lellouche et al., 2021; Zuo et al., 2019). Advances in ocean reanalyses assimilation methods may also contribute to the improved consistency among products. These developments can help observations

https://doi.org/10.5194/egusphere-2026-6613
Preprint. Discussion started: 3 November 2026
© Author(s) 2026. CC BY 4.0 License.

constrain model states in a more physically consistent way. However, the improvement is strongly depth dependent: agreement increases mainly in the upper 2000 m, while no comparable improvement is found in the 2000–5000 m layer. This contrast suggests that methodological and ocean model advances alone cannot explain the post-2005 increase in agreement, and that the enhanced observational constraint provided by the Argo observing system is likely a more important factor.

Some observations have detected deep-ocean warming, particularly in the Southern Ocean and along the Antarctic Bottom Water circulation pathway (Desbruyères et al., 2016; Johnson and Purkey, 2024; Purkey and Johnson, 2010). However, they do not yet provide the sustained, near-global sampling needed to tightly constrain ORA-based OHC changes below 2000 m. In regions where observational data are available, these data can be used to assess whether ORAs reproduce observed deep-ocean water mass characteristics and temperature changes. In regions lacking sufficient observational constraints, reanalyses-based estimates of OHC in the 2000–5000 m layer should be interpreted with caution, as should the OAs.

Agreement among ORAs and OAs still remains weak in some regions in the upper 2000 m. These regions are mainly located in the Arctic Ocean, the middle and high latitudes of the Southern Ocean, and dynamically active current systems and frontal zones. In polar oceans, sparse observations are an important source of uncertainty, but they are not the only source. Reanalyses results in these regions also depend strongly on the model parameterizations, atmospheric forcing, and data assimilation schemes. This is because high-latitude OHC is controlled by tightly coupled ocean and sea ice processes, heat transport through strait gateways, complex vertical mixing, as well as ocean circulation (Eisner et al., 2025, 2026a, b; Josey et al., 2024; Muilwijk et al., 2024; Nie et al., 2023; Zhang et al., 2023, 2025). Additional observations are needed to further constrain the range of acceptable solutions. These processes are difficult to represent consistently across different ocean models (Allende et al., 2024; Uotila et al., 2019). The seasonal-amplitude analysis further shows that ORA uncertainty in most regions is not limited to long-term trends, but also affects the representation of seasonal heat storage and redistribution. Therefore, seasonal-to-interannual OHC studies should include multi-product uncertainty assessment.

https://doi.org/10.5194/egusphere-2026-6613
Preprint. Discussion started: 3 November 2026
© Author(s) 2026. CC BY 4.0 License.

These regional uncertainties have direct implications for climate studies that use ORAs and OAs. For example, in the Arctic Ocean, upper-ocean heat anomalies influence sea ice growth, melt, and variability. Weak constraints on Arctic upper-ocean OHC may therefore affect estimates of the oceanic contribution to sea ice variability and ice loss. The Southern Ocean is a major region of global ocean heat uptake and interior heat storage (Armour et al., 2016; Huguenin et al., 2022). Uncertainty in this region can influence estimates of global ocean heat uptake efficiency, interior heat storage, and thermosteric sea-level change (Palmer et al., 2017). Therefore, relying on a single ORA or OA product in these regions that lack observations can lead to product-dependent interpretations of the sea-ice–OHC relationship, Southern Ocean heat-uptake efficiency, and the thermosteric sea-level contribution. The ensemble mean of ocean reanalyses could be a better choice for these climate studies. A parallel study of the polar region within MER-EP is ongoing, as well which will provide more details about the performances of ocean reanalyses in polar regions.

Maintaining and strengthening the global ocean observing system is essential for improving OHC estimates. The post-2005 improvement found here is consistent with observing-system degradation experiments by Zhu et al., (2026), which show that a reduction in observations would weaken the monitoring of OHC. Our study did not conduct comparable observation-denial experiments for individual reanalyses systems, and therefore cannot isolate the causal contribution of observations to each ORA product. Nevertheless, the depth-dependent improvement supports the need for sustained, stable, and high-quality ocean observations. Future studies should use observing system experiments to quantify the impacts of Argo, Deep Argo, satellite altimetry, and polar observations on different reanalyses systems. Such experiments would help identify the most important observational gaps and guide future sampling priorities.

The comparison between the outcome of this activity (MER-EP) and the last intercomparison effort (ORA-IP) shows clear evidence that the latest generation of ocean reanalyses products are improved. These improvements likely reflect a combination of model resolution, advances in model physics, and improved data assimilation methods. However, further improvement is also needed in reanalyses systems themselves, especially in the treatment of systematic model bias, model drift, and analysis adjustments

https://doi.org/10.5194/egusphere-2026-6613
Preprint. Discussion started: 3 November 2026
© Author(s) 2026. CC BY 4.0 License.

associated with changes in the assimilated observing network. Optimizing model parameterizations can notably provide a path to reducing model drifts, but this requires an adjoint to propagate data constraints over multidecadal time scales (Forget et al., 2015a, b).

Model drift can be particularly important for the pre-Argo period, when subsurface temperature and salinity profiles were sparse and unevenly distributed, making OHC estimates more dependent on the model background, surface forcing, initialization, and bias correction. For example, ORAS4 used an Argo-period estimate of model bias and applied it retrospectively, and its sensitivity experiment without bias correction showed that bias correction affects the magnitude and timing of OHC changes, especially in the 700–2000 m layer (Balmaseda et al., 2013a). ORAS5 further estimated the a priori bias from Argo-era ensemble assimilation runs to reduce spurious climate signals associated with the evolving observing network (Zuo et al., 2019). Assimilation experiments also show that sparse pre-Argo profile data can produce analysis shocks, whereas these shocks are greatly reduced when near-global Argo profiles are assimilated (Sivareddy et al., 2017). Bias and drift correction strategies that are constrained using the better-observed Argo period and applied to earlier decades may therefore improve the consistency of pre-Argo estimates and help limit the magnitude of analysis shocks when Argo observations are introduced.

The regions with weak agreement identified in this study also indicate where model development is most needed. WBC and frontal zones require higher resolution and better representation of mesoscale and submesoscale variability. Polar oceans require improved sea ice–ocean coupling, regional circulation, and vertical mixing. For the 2000–5000 m layer, controlling model drift remains essential. The requirements for next-generation ocean reanalyses summarized by Yang et al., (2025) also emphasize higher spatial resolution, transparent uncertainty assessment, unified evaluation metrics, and application-oriented diagnostic variables. For OHC studies, this means that future ORAs should provide not only temperature and salinity fields, but also heat budget terms (Forget et al., 2015a; Forget and Ferreira, 2019; Jiang et al., 2026; Song and Forget, 2026), assimilation increments, and uncertainty quantification.

https://doi.org/10.5194/egusphere-2026-6613
Preprint. Discussion started: 3 November 2026
© Author(s) 2026. CC BY 4.0 License.

5 Concluding remarks

Within the MER-EP framework, this study evaluates the ability of 13 new-generation ocean reanalyses products to represent changes in OHC since 1993. The assessment focuses on large-scale OHC trends, changes in inter-product consistency before and after the implementation of the Argo observing system, the depth and regional dependence of reanalyses uncertainty, and whether the new-generation products show improved consistency in representing OHC compared with earlier-generation reanalyses. This study mainly reached the following conclusions:

1) Most ORAs and OAs consistently show sustained ocean warming during 1993–2022, particularly in the upper 2000 m. The ORA EM gives a global 0–2000 m OHC trend of 0.73 [0.49, 0.97] W m^{-2} ($\pm$1.65 std), with trend estimates from the OAs falling within the ORA uncertainty range. Over 2005–2023, the estimated upper-2000 m ocean heating rate trends were 0.29 [−0.21, 0.80] W m^{-2} $decade^{-1}$ for ORA EM and 0.26 [0.10, 0.37] W m^{-2} $decade^{-1}$ for IAPv4; both central estimates were lower than the corresponding CERES net TOA radiation trend of 0.54 W m^{-2} $decade^{-1}$.

2) Ocean warming since 1993 shows a clear large-scale spatial and vertical pattern. Horizontally, pronounced warming occurs in the Atlantic, North Pacific, Indian Ocean, western Pacific, and most of the Southern Ocean, while cooling is mainly found in the subpolar North Atlantic, eastern equatorial Pacific, and parts of the Southern Ocean near the Subantarctic and Polar Fronts. In the latitude–depth structure, warming is concentrated mainly within the upper 2000 m and is strongest at mid-latitudes, with warming extending to greater depths at high northern latitudes than in the Southern Hemisphere; below about 2000 m, temperature trends are generally much weaker at global scale.

3) Agreement among ORAs improves markedly after the transition to the Argo era. For interannual variability, the fraction of ocean area with S/N > 1 in the 0–2000 m layer increases from 52.9% during 1993–2004 to 73.7% during 2005–2022; for OHC trends, it increases from 44.2% to 65.5%. The largest improvement occurs in the 700–2000 m layer, whereas little improvement is found below 2000 m. This result highlights the importance of sustained development and long-term maintenance of the global ocean observing system for constraining OHC estimates.

https://doi.org/10.5194/egusphere-2026-6613
Preprint. Discussion started: 3 November 2026
© Author(s) 2026. CC BY 4.0 License.

4) The recent-generation ORAs used in MER-EP show greater internal consistency than the earlier ORA-IP products over their common 1993–2010 period. In the upper 1500 m, the MER-EP ORA ensemble has S/N > 1 over 59.9% of the ocean for interannual variability, compared with the ORA-IP mean of 48.6%. For trends, the corresponding values are 54.9% for MER-EP versus the ORA-IP mean of 31.2%.

5) Large uncertainties remain in the deep ocean and in dynamically complex or poorly observed regions (low confidence). OHC estimates are strongly product dependent in the 2000–5000 m layer, polar oceans, WBC and ACC/frontal systems. Analyses in these regions therefore require explicit multi-product uncertainty assessment rather than reliance on a single ORA.

Code and data availability

IAPv4 OHC data were obtained from the Institute of Atmospheric Physics, Chinese Academy of Sciences, at https://doi.org/10.12157/IOCAS.20240117.001. EN4 temperature and salinity data were obtained from the Met Office Hadley Centre at https://www.metoffice.gov.uk/hadobs/en4/download.html. Ishii temperature and OHC data were obtained from the Japan Meteorological Agency at https://www.data.jma.go.jp/kaiyou/english/ohc/ohc_data_en.html. NCEI OHC data were obtained from NOAA National Centers for Environmental Information at https://www.ncei.noaa.gov/access/global-ocean-heat-content/. GOHC data were obtained from the data archive at https://doi.org/10.5281/zenodo.18485246. GCOS OHC data were obtained from the World Data Center for Climate at https://doi.org/10.26050/WDCC/GCOS_EHI_1960-2020_OHC_v2. ORAS5 data were obtained from the Copernicus Climate Data Store at https://cds.climate.copernicus.eu/datasets/reanalysis-oras5. BRAN2020 data were obtained from the Australian National Computational Infrastructure at https://doi.org/10.25914/6009627c7af03. SODA3 data were obtained from the University of Maryland SODA project at https://www.soda.umd.edu/soda3/. ESTOC data were obtained from JAMSTEC at https://www.jamstec.go.jp/estoc/e/index.html. GODAS data were obtained from NOAA Physical Sciences Laboratory at https://psl.noaa.gov/data/gridded/data.godas.html. C-GLORSv7, GLORYS2v4 and GLORYS12v1 data were obtained from https://data.marine.copernicus.eu/product/GLOBAL_MULTIYEAR_PHY_ENS_001_031/description.

https://doi.org/10.5194/egusphere-2026-6613
Preprint. Discussion started: 3 November 2026
© Author(s) 2026. CC BY 4.0 License.

CERES EBAF data were obtained from the NASA CERES data archive at https://ceres.larc.nasa.gov/data/. The processed data from C-GLORSv8, CIGAR025, CIGAR1, GLORYS4v2, and GloSia9-1 used to generate the figures in this study will be made publicly available upon publication.

Author contributions

H.Z. analyzed the data, produced the figures, and wrote the original draft. C.Y., R.B., A.S., and L.C. conceptualized the study. All authors contributed to the review and editing of the paper.

Acknowledgments

This research was supported by the Copernicus Marine Service Global Reanalyses Lot 1 project (24254-COP-GLORAN-4000), the "CAS Project for Young Scientists in Basic Research" (No. YSBR-137), the International Partnership Program of the Chinese Academy of Sciences (Grant No. 060GJHZ2024064MI), the Chinese Academy of Sciences and the National Research Council of Italy Scientific Cooperative Program. Thank Richard Renshaw (UK Met Office) for providing us the GloSia9-1 data.

References

Allende, S., Treguier, A. M., Lique, C., de Boyer Montégut, C., Massonnet, F., Fichefet, T., and Barthélemy, A.: Impact of ocean vertical-mixing parameterization on Arctic sea ice and upper-ocean properties using the NEMO-SI3 model, Geoscientific Model Development, 17, 7445–7466, https://doi.org/10.5194/gmd-17-7445-2024, 2024.

Armour, K. C., Marshall, J., Scott, J. R., Donohoe, A., and Newsom, E. R.: Southern Ocean warming delayed by circumpolar upwelling and equatorward transport, Nature Geoscience, 9, 549–554, https://doi.org/10.1038/ngeo2731, 2016.

https://doi.org/10.5194/egusphere-2026-6613
Preprint. Discussion started: 3 November 2026
© Author(s) 2026. CC BY 4.0 License.

Balmaseda, M. A., Trenberth, K. E., and Källén, E.: Distinctive climate signals in reanalysis of global ocean heat content, Geophysical Research Letters, 40, 1754–1759, https://doi.org/10.1002/grl.50382, 2013a.

Balmaseda, M. A., Mogensen, K., and Weaver, A. T.: Evaluation of the ECMWF ocean reanalysis system ORAS4, Quarterly Journal of the Royal Meteorological Society, 139, 1132–1161, https://doi.org/10.1002/qj.2063, 2013b.

Bouih, M., Barnoud, A., Yang, C., Storto, A., Blazquez, A., Llovel, W., Fraudeau, R., and Cazenave, A.: Regional sea level trend budget over 2004–2022, Ocean Science, 21, 1425–1440, https://doi.org/10.5194/os-21-1425-2025, 2025.

Bourdallé-Badie, R., Lellouche, J.-M., Greiner, E., Hamon, M., Ruggiero, G., Le Galloudec, O., Testut, C.-E., Benkiran, M., Garric, G., Drévillon, M., Parent, L., and Melet, A.: OSM2026_poster_RBB_GLORYS4V2_v1.0, , https://doi.org/10.5281/zenodo.23045545, 2026.

Boyer, T., Domingues, C. M., Good, S. A., Johnson, G. C., Lyman, J. M., Ishii, M., Gouretski, V., Willis, J. K., Antonov, J., Wijffels, S., Church, J. A., Cowley, R., and Bindoff, N. L.: Sensitivity of Global Upper-Ocean Heat Content Estimates to Mapping Methods, XBT Bias Corrections, and Baseline Climatologies, Journal of Climate, 29, 4817–4842, https://doi.org/10.1175/jcli-d-15-0801.1, 2016.

Carton, J. A., Chepurin, G. A., and Chen, L.: SODA3: A New Ocean Climate Reanalysis, Journal of Climate, 31, 6967–6983, https://doi.org/10.1175/jcli-d-18-0149.1, 2018.

Chamberlain, M. A., Oke, P. R., Fiedler, R. A. S., Beggs, H. M., Brassington, G. B., and Divakaran, P.: Next generation of Bluelink ocean reanalysis with multiscale data assimilation: BRAN2020, Earth System Science Data, 13, 5663–5688, https://doi.org/10.5194/essd-13-5663-2021, 2021.

Chassignet, E. P. and Xu, X.: Impact of Horizontal Resolution (1/12° to 1/50°) on Gulf Stream Separation, Penetration, and Variability, Journal of Physical Oceanography, 47, 1999–2021, https://doi.org/10.1175/jpo-d-17-0031.1, 2017.

https://doi.org/10.5194/egusphere-2026-6613
Preprint. Discussion started: 3 November 2026
© Author(s) 2026. CC BY 4.0 License.

Cheng, L., von Schuckmann, K., Abraham, J. P., Trenberth, K. E., Mann, M. E., Zanna, L., England, M. H., Zika, J. D., Fasullo, J. T., Yu, Y., Pan, Y., Zhu, J., Newsom, E. R., Bronselaer, B., and Lin, X.: Past and future ocean warming, Nat Rev Earth Environ, 3, 776–794, https://doi.org/10.1038/s43017-022-00345-1, 2022.

Cheng, L., Pan, Y., Tan, Z., Zheng, H., Zhu, Y., Wei, W., Du, J., Yuan, H., Li, G., Ye, H., Gouretski, V., Li, Y., Trenberth, K. E., Abraham, J., Jin, Y., Reseghetti, F., Lin, X., Zhang, B., Chen, G., Mann, M. E., and Zhu, J.: IAPv4 ocean temperature and ocean heat content gridded dataset, Earth Syst. Sci. Data, 16, 3517–3546, https://doi.org/10.5194/essd-16-3517-2024, 2024.

Copernicus Marine Service: Global Ocean Sea Surface Temperature time series and trend from Observations Reprocessing, https://doi.org/10.48670/MOI-00242, 2025.

Desbruyères, D. G., Purkey, S. G., McDonagh, E. L., Johnson, G. C., and King, B. A.: Deep and abyssal ocean warming from 35 years of repeat hydrography, Geophysical Research Letters, 43, 10356–10365, https://doi.org/10.1002/2016gl070413, 2016.

Drévillon, M., Lellouche, J.-M., Régnier, C., Garric, G., Bricaud, C., Hernandez, O., and Bourdallé-Badie, R.: Quality Information Document for Global Ocean Reanalysis Products GLOBAL_REANALYSIS_PHY_001_030, Quality Information Document, CMEMS-GLO-QUID-001-030, Mercator Ocean International, Toulouse, France, https://documentation.marine.copernicus.eu/QUID/CMEMS-GLO-QUID-001-030.pdf (last access: 1 October 2026), 2023.

Eisner, S. A., Carton, J. A., and Chafik, L.: Atlantic Water Heat Transport Variability and Trends Into the Amerasian Basin: A First Look Using SODA4, Journal of Geophysical Research: Oceans, 130, e2025JC023382, https://doi.org/10.1029/2025jc023382, 2025.

Eisner, S. A., Carton, J. A., Chafik, L., and Smedsrud, L. H.: Increased ocean heat transport to the central Arctic despite a well working Barents Sea Cooling Machine, Ocean Science, 22, 1073–1084, https://doi.org/10.5194/os-22-1073-2026, 2026a.

https://doi.org/10.5194/egusphere-2026-6613
Preprint. Discussion started: 3 November 2026
© Author(s) 2026. CC BY 4.0 License.

Eisner, S. A., Chafik, L., Steele, M., and Carton, J. A.: Long-Term Trends and Variability in Arctic Mixed Layer Depth, Journal of Geophysical Research: Oceans, 131, e2026JC024063, https://doi.org/10.1029/2026jc024063, 2026b.

Flato, G., Marotzke, J., Abiodun, B., Braconnot, P., Chou, S. C., Collins, W., Cox, P., Driouech, F., Emori, S., Eyring, V., Forest, C., Gleckler, P., Guilyardi, E., Jakob, C., Kattsov, V., Reason, C., and Rummukainen, M.: Evaluation of Climate Models, in: Climate Change 2013: The Physical Science Basis, edited by: Stocker, T. F., Qin, D., Plattner, G.-K., Tignor, M., Allen, S. K., Boschung, J., Nauels, A., Xia, Y., Bex, V., and Midgley, P. M., Cambridge University Press, Cambridge, UK and New York, NY, USA, 741–866, https://doi.org/10.1017/cbo9781107415324.020, 2013.

Forget, G.: Mapping Ocean Observations in a Dynamical Framework: A 2004–06 Ocean Atlas, Journal of Physical Oceanography, 40, 1201–1221, https://doi.org/10.1175/2009jpo4043.1, 2010.

Forget, G.: Ocean Heat Transport Convergence Drives Regional Energy Imbalance in the Sunlit Ocean Layer, https://doi.org/10.5194/egusphere-2026-4643, 2026., 2026.

Forget, G. and Ferreira, D.: Global ocean heat transport dominated by heat export from the tropical Pacific, Nature Geoscience, 12, 351–354, https://doi.org/10.1038/s41561-019-0333-7, 2019.

Forget, G. and Ponte, R. M.: The partition of regional sea level variability, Progress in Oceanography, 137, 173–195, https://doi.org/10.1016/j.pocean.2015.06.002, 2015.

Forget, G., Campin, J.-M., Heimbach, P., Hill, C. N., Ponte, R. M., and Wunsch, C.: ECCO version 4: an integrated framework for non-linear inverse modeling and global ocean state estimation, Geosci. Model Dev., 8, 3071–3104, https://doi.org/10.5194/gmd-8-3071-2015, 2015a.

Forget, G., Ferreira, D., and Liang, X.: On the observability of turbulent transport rates by Argo: supporting evidence from an inversion experiment, Ocean Science, 11, 839–853, https://doi.org/10.5194/os-11-839-2015, 2015b.

https://doi.org/10.5194/egusphere-2026-6613
Preprint. Discussion started: 3 November 2026
© Author(s) 2026. CC BY 4.0 License.

Fox-Kemper, B., Hewitt, H. T., Xiao, C., Aðalgeirsdóttir, G., Drijfhout, S. S., Edwards, T. L., Golledge, N. R., Hemer, M., Kopp, R. E., Krinner, G., Mix, A., Notz, D., Nowicki, S., Nurhati, I. S., Ruiz, L., Sallée, J.-B., Slangen, A. B. A., and Yu, Y.: Ocean, Cryosphere and Sea Level Change, in: Climate Change 2021: The Physical Science Basis, edited by: Masson-Delmotte, V., Zhai, P., Pirani, A., Connors, S. L., Péan, C., Berger, S., Caud, N., Chen, Y., Goldfarb, L., Gomis, M. I., Huang, M., Leitzell, K., Lonnoy, E., Matthews, J. B. R., Maycock, T. K., Waterfield, T., Yelekçi, Ö., Yu, R., and Zhou, B., Cambridge University Press, Cambridge, UK and New York, NY, USA, 1211–1362, https://doi.org/10.1017/9781009157896.011, 2021.

Good, S. A., Martin, M. J., and Rayner, N. A.: EN4: Quality controlled ocean temperature and salinity profiles and monthly objective analyses with uncertainty estimates, Journal of Geophysical Research: Oceans, 118, 6704–6716, https://doi.org/10.1002/2013jc009067, 2013.

Guiavarc'h, C., Storkey, D., Blaker, A. T., Blockley, E., Megann, A., Hewitt, H., Bell, M. J., Calvert, D., Copsey, D., Sinha, B., Moreton, S., Mathiot, P., and An, B.: GOSI9: UK Global Ocean and Sea Ice configurations, Geoscientific Model Development, 18, 377–403, https://doi.org/10.5194/gmd-18-377-2025, 2025.

Hakuba, M. Z., Fourest, S., Boyer, T., Meyssignac, B., Carton, J. A., Forget, G., Cheng, L., Giglio, D., Johnson, G. C., Kato, S., Killick, R. E., Kolodziejczyk, N., Kuusela, M., Landerer, F., Llovel, W., Locarnini, R., Loeb, N., Lyman, J. M., Mishonov, A., Pilewskie, P., Reagan, J., Storto, A., Sukianto, T., and von Schuckmann, K.: Trends and Variability in Earth's Energy Imbalance and Ocean Heat Uptake Since 2005, Surv Geophys, 45, 1721–1756, https://doi.org/10.1007/s10712-024-09849-5, 2024.

Heimbach, P., Fukumori, I., Hill, C. N., Ponte, R. M., Stammer, D., Wunsch, C., Campin, J.-M., Cornuelle, B., Fenty, I., Forget, G., Köhl, A., Mazloff, M., Menemenlis, D., Nguyen, A. T., Piecuch, C., Trossman, D., Verdy, A., Wang, O., and Zhang, H.: Putting It All Together: Adding Value to the Global Ocean and Climate Observing Systems With Complete Self-Consistent Ocean State and Parameter Estimates, Frontiers in Marine Science, 6, 55, https://doi.org/10.3389/fmars.2019.00055, 2019.

https://doi.org/10.5194/egusphere-2026-6613
Preprint. Discussion started: 3 November 2026
© Author(s) 2026. CC BY 4.0 License.

Huang, B., Xue, Y., and Behringer, D. W.: Impacts of Argo salinity in NCEP Global Ocean Data Assimilation System: The tropical Indian Ocean, J. Geophys. Res., 113, C08002, https://doi.org/10.1029/2007jc004388, 2008.

Huguenin, M. F., Holmes, R. M., and England, M. H.: Drivers and distribution of global ocean heat uptake over the last half century, Nat Commun, 13, 4921, https://doi.org/10.1038/s41467-022-32540-5, 2022.

Intergovernmental Oceanographic Commission, Scientific Committee on Oceanic Research, and International Association for the Physical Sciences of the Oceans: The international thermodynamic equation of seawater – 2010: Calculation and use of thermodynamic properties, Manuals and Guides, IOC/2010/MG/56, Intergovernmental Oceanographic Commission, UNESCO, Paris, https://www.teos-10.org/pubs/TEOS-10_Manual.pdf (last access: 1 October 2026), 2010.

Ishii, M., Fukuda, Y., Hirahara, S., Yasui, S., Suzuki, T., and Sato, K.: Accuracy of Global Upper Ocean Heat Content Estimation Expected from Present Observational Data Sets, SOLA, 13, 163–167, https://doi.org/10.2151/sola.2017-030, 2017.

Jackson, L. C., Dubois, C., Forget, G., Haines, K., Harrison, M., Iovino, D., Köhl, A., Mignac, D., Masina, S., Peterson, K. A., Piecuch, C. G., Roberts, C. D., Robson, J., Storto, A., Toyoda, T., Valdivieso, M., Wilson, C., Wang, Y., and Zuo, H.: The Mean State and Variability of the North Atlantic Circulation: A Perspective From Ocean Reanalyses, Journal of Geophysical Research: Oceans, 124, 9141–9170, https://doi.org/10.1029/2019jc015210, 2019.

Jiang, W., Forget, G., Song, Y., and Haine, T. W. N.: Coupled air–sea interactions drove and sustained the 2013–2016 North Pacific marine heatwave, Nature Communications, 17, 9396, https://doi.org/10.1038/s41467-026-76096-0, 2026.

Johnson, G. C. and Purkey, S. G.: Refined Estimates of Global Ocean Deep and Abyssal Decadal Warming Trends, Geophysical Research Letters, 51, e2024GL111229, https://doi.org/10.1029/2024gl111229, 2024.

https://doi.org/10.5194/egusphere-2026-6613
Preprint. Discussion started: 3 November 2026
© Author(s) 2026. CC BY 4.0 License.

Johnson, G. C., Hosoda, S., Jayne, S. R., Oke, P. R., Riser, S. C., Roemmich, D., Suga, T., Thierry, V., Wijffels, S. E., and Xu, J.: Argo—Two Decades: Global Oceanography, Revolutionized, Annual Review of Marine Science, 14, 379–403, https://doi.org/10.1146/annurev-marine-022521-102008, 2022.

Johnson, G. C., Landerer, F. W., Loeb, N. G., Lyman, J. M., Mayer, M., Swann, A. L. S., and Zhang, J.: Closure of Earth's Global Seasonal Cycle of Energy Storage, Surveys in Geophysics, 45, 1785–1797, https://doi.org/10.1007/s10712-023-09797-6, 2024.

Josey, S. A., Meijers, A. J. S., Blaker, A. T., Grist, J. P., Mecking, J., and Ayres, H. C.: Record-low Antarctic sea ice in 2023 increased ocean heat loss and storms, Nature, 636, 635–639, https://doi.org/10.1038/s41586-024-08368-y, 2024.

Killick, R.: EN.4.2.2 Product User Guide, version 1.0, Met Office Hadley Centre, https://www.metoffice.gov.uk/hadobs/en4/EN.4.2.2_Product_User_Guide_v1.0.pdf, 2021.

Lellouche, J.-M., Le Galloudec, O., Drévillon, M., Régnier, C., Greiner, E., Garric, G., Ferry, N., Desportes, C., Testut, C.-E., Bricaud, C., Bourdallé-Badie, R., Tranchant, B., Benkiran, M., Drillet, Y., Daudin, A., and De Nicola, C.: Evaluation of global monitoring and forecasting systems at Mercator Océan, Ocean Science, 9, 57–81, https://doi.org/10.5194/os-9-57-2013, 2013.

Lellouche, J.-M., Greiner, E., Le Galloudec, O., Garric, G., Regnier, C., Drevillon, M., Benkiran, M., Testut, C.-E., Bourdalle-Badie, R., Gasparin, F., Hernandez, O., Levier, B., Drillet, Y., Remy, E., and Le Traon, P.-Y.: Recent updates to the Copernicus Marine Service global ocean monitoring and forecasting real-time 1⁄12° high-resolution system, Ocean Science, 14, 1093–1126, https://doi.org/10.5194/os-14-1093-2018, 2018.

Lellouche, J.-M., Greiner, E., Bourdallé-Badie, R., Garric, G., Melet, A., Drévillon, M., Bricaud, C., Hamon, M., Le Galloudec, O., Régnier, C., Candela, T., Testut, C.-E., Gasparin, F., Ruggiero, G., Benkiran, M., Drillet, Y., and Le Traon, P.-Y.: The Copernicus Global 1/12° Oceanic and Sea Ice GLORYS12 Reanalysis, Frontiers in Earth Science, 9, 698876, https://doi.org/10.3389/feart.2021.698876, 2021.

https://doi.org/10.5194/egusphere-2026-6613
Preprint. Discussion started: 3 November 2026
© Author(s) 2026. CC BY 4.0 License.

Levitus, S., Antonov, J. I., Boyer, T. P., Baranova, O. K., Garcia, H. E., Locarnini, R. A., Mishonov, A. V., Reagan, J. R., Seidov, D., Yarosh, E. S., and Zweng, M. M.: World ocean heat content and thermosteric sea level change (0–2000 m), 1955–2010, Geophysical Research Letters, 39, L10603, https://doi.org/10.1029/2012gl051106, 2012.

Liang, X., Liu, C., Ponte, R. M., and Chambers, D. P.: A Comparison of the Variability and Changes in Global Ocean Heat Content from Multiple Objective Analysis Products During the Argo Period, Journal of Climate, 34, 7875–7895, https://doi.org/10.1175/jcli-d-20-0794.1, 2021.

Liu, C., Jin, L., Cao, N., Su, Q., Cheng, L., Liao, X., Allan, R. P., Qiao, F., Song, Z., Mayer, M., Winkelbauer, S., Li, J., Xu, H., Yang, K., Pan, Y., and Liang, Z.: Assessment of the global ocean heat content and North Atlantic heat transport over 1993–2020, npj Climate and Atmospheric Science, 7, 314, https://doi.org/10.1038/s41612-024-00860-6, 2024.

Loeb, N. G., Johnson, G. C., Thorsen, T. J., Lyman, J. M., Rose, F. G., and Kato, S.: Satellite and Ocean Data Reveal Marked Increase in Earth's Heating Rate, Geophysical Research Letters, 48, e2021GL093047, https://doi.org/10.1029/2021gl093047, 2021.

Ludwigsen, C. B., Andersen, O. B., Marzeion, B., Malles, J.-H., Müller Schmied, H., Döll, P., Watson, C., and King, M. A.: Global and regional ocean mass budget closure since 2003, Nature Communications, 15, 1416, https://doi.org/10.1038/s41467-024-45726-w, 2024.

MacLachlan, C., Arribas, A., Peterson, K. A., Maidens, A., Fereday, D., Scaife, A. A., Gordon, M., Vellinga, M., Williams, A., Comer, R. E., Camp, J., Xavier, P., and Madec, G.: Global Seasonal forecast system version 5 (GloSea5): a high-resolution seasonal forecast system, Quarterly Journal of the Royal Meteorological Society, 141, 1072–1084, https://doi.org/10.1002/qj.2396, 2015.

Marti, F., Blazquez, A., Meyssignac, B., Ablain, M., Barnoud, A., Fraudeau, R., Jugier, R., Chenal, J., Larnicol, G., Pfeffer, J., Restano, M., and Benveniste, J.: Monitoring the ocean heat content change and the Earth energy imbalance from space altimetry and space gravimetry, Earth System Science Data, 14, 229–249, https://doi.org/10.5194/essd-14-229-2022, 2022.

https://doi.org/10.5194/egusphere-2026-6613
Preprint. Discussion started: 3 November 2026
© Author(s) 2026. CC BY 4.0 License.

Menemenlis, D., Campin, J.-M., Heimbach, P., Hill, C., Lee, T., Nguyen, A., Schodlok, M., and Zhang, H.: ECCO2: High resolution global ocean and sea ice data synthesis, , Mercator Ocean Quarterly Newsletter13–21, 2008.

Meyssignac, B., Boyer, T., Zhao, Z., Hakuba, M. Z., Landerer, F. W., Stammer, D., Köhl, A., Kato, S., L'Ecuyer, T., Ablain, M., Abraham, J. P., Blazquez, A., Cazenave, A., Church, J. A., Cowley, R., Cheng, L., Domingues, C. M., Giglio, D., Gouretski, V., Ishii, M., Johnson, G. C., Killick, R. E., Legler, D., Llovel, W., Lyman, J., Palmer, M. D., Piotrowicz, S., Purkey, S. G., Roemmich, D., Roca, R., Savita, A., von Schuckmann, K., Speich, S., Stephens, G., Wang, G., Wijffels, S. E., and Zilberman, N.: Measuring Global Ocean Heat Content to Estimate the Earth Energy Imbalance, Frontiers in Marine Science, 6, 432, https://doi.org/10.3389/fmars.2019.00432, 2019.

Minière, A., von Schuckmann, K., Sallée, J.-B., and Vogt, L.: Robust acceleration of Earth system heating observed over the past six decades, Scientific Reports, 13, 22975, https://doi.org/10.1038/s41598-023-49353-1, 2023.

Minière, A., von Schuckmann, K., and Speich, S.: Consolidating Global Estimates of Ocean Heat Content: Toward a Consistent Earth Heat Inventory, https://doi.org/10.5194/essd-2026-106, 2026., 2026.

Muilwijk, M., Hattermann, T., Martin, T., and Granskog, M. A.: Future sea ice weakening amplifies wind-driven trends in surface stress and Arctic Ocean spin-up, Nature Communications, 15, 6889, https://doi.org/10.1038/s41467-024-50874-0, 2024.

Nie, Y., Li, C., Vancoppenolle, M., Cheng, B., Boeira Dias, F., Lv, X., and Uotila, P.: Sensitivity of NEMO4.0-SI^3 model parameters on sea ice budgets in the Southern Ocean, Geoscientific Model Development, 16, 1395–1425, https://doi.org/10.5194/gmd-16-1395-2023, 2023.

Osafune, S., Masuda, S., Sugiura, N., and Doi, T.: Evaluation of the applicability of the Estimated State of the Global Ocean for Climate Research (ESTOC) data set, Geophysical Research Letters, 42, 4903–4911, https://doi.org/10.1002/2015gl064538, 2015.

https://doi.org/10.5194/egusphere-2026-6613
Preprint. Discussion started: 3 November 2026
© Author(s) 2026. CC BY 4.0 License.

Palmer, M. D., Roberts, C. D., Balmaseda, M., Chang, Y.-S., Chepurin, G., Ferry, N., Fujii, Y., Good, S. A., Guinehut, S., Haines, K., Hernandez, F., Köhl, A., Lee, T., Martin, M. J., Masina, S., Masuda, S., Peterson, K. A., Storto, A., Toyoda, T., Valdivieso, M., Vernieres, G., Wang, O., and Xue, Y.: Ocean heat content variability and change in an ensemble of ocean reanalyses, Clim Dyn, 49, 909–930, https://doi.org/10.1007/s00382-015-2801-0, 2017.

Pan, Y., Cheng, L., von Schuckmann, K., Trenberth, K. E., Li, G., Abraham, J., Liu, Y., Gouretski, V., Yu, Y., Liu, H., and Liu, C.: Annual Cycle in Upper-Ocean Heat Content and the Global Energy Budget, Journal of Climate, 36, 5003–5026, https://doi.org/10.1175/jcli-d-22-0776.1, 2023.

Purkey, S. G. and Johnson, G. C.: Warming of Global Abyssal and Deep Southern Ocean Waters between the 1990s and 2000s: Contributions to Global Heat and Sea Level Rise Budgets, Journal of Climate, 23, 6336–6351, https://doi.org/10.1175/2010jcli3682.1, 2010.

Riser, S. C., Freeland, H. J., Roemmich, D., Wijffels, S., Troisi, A., Belbéoch, M., Gilbert, D., Xu, J., Pouliquen, S., Thresher, A., Le Traon, P.-Y., Maze, G., Klein, B., Ravichandran, M., Grant, F., Poulain, P.-M., Suga, T., Lim, B., Sterl, A., Sutton, P., Mork, K.-A., Vélez-Belchí, P. J., Ansorge, I., King, B., Turton, J., Baringer, M., and Jayne, S. R.: Fifteen years of ocean observations with the global Argo array, Nature Climate Change, 6, 145–153, https://doi.org/10.1038/nclimate2872, 2016.

von Schuckmann, K., Cheng, L., Palmer, M. D., Hansen, J., Tassone, C., Aich, V., Adusumilli, S., Beltrami, H., Boyer, T., Cuesta-Valero, F. J., Desbruyères, D., Domingues, C., García-García, A., Gentine, P., Gilson, J., Gorfer, M., Haimberger, L., Ishii, M., Johnson, G. C., Killick, R., King, B. A., Kirchengast, G., Kolodziejczyk, N., Lyman, J., Marzeion, B., Mayer, M., Monier, M., Monselesan, D. P., Purkey, S., Roemmich, D., Schweiger, A., Seneviratne, S. I., Shepherd, A., Slater, D. A., Steiner, A. K., Straneo, F., Timmermans, M.-L., and Wijffels, S. E.: Heat stored in the Earth system: where does the energy go?, Earth System Science Data, 12, 2013–2041, https://doi.org/10.5194/essd-12-2013-2020, 2020.

von Schuckmann, K., Minière, A., Gues, F., Cuesta-Valero, F. J., Kirchengast, G., Adusumilli, S., Straneo, F., Ablain, M., Allan, R. P., Barker, P. M., Beltrami, H., Blazquez, A., Boyer, T., Cheng, L., Church, J.,

https://doi.org/10.5194/egusphere-2026-6613
Preprint. Discussion started: 3 November 2026
© Author(s) 2026. CC BY 4.0 License.

Desbruyeres, D., Dolman, H., Domingues, C. M., García-García, A., Giglio, D., Gilson, J. E., Gorfer, M., Haimberger, L., Hakuba, M. Z., Hendricks, S., Hosoda, S., Johnson, G. C., Killick, R., King, B., Kolodziejczyk, N., Korosov, A., Krinner, G., Kuusela, M., Landerer, F. W., Langer, M., Lavergne, T., Lawrence, I., Li, Y., Lyman, J., Marti, F., Marzeion, B., Mayer, M., MacDougall, A. H., McDougall, T., Monselesan, D. P., Nitzbon, J., Otosaka, I., Peng, J., Purkey, S., Roemmich, D., Sato, K., Sato, K., Savita, A., Schweiger, A., Shepherd, A., Seneviratne, S. I., Simons, L., Slater, D. A., Slater, T., Steiner, A. K., Suga, T., Szekely, T., Thiery, W., Timmermans, M.-L., Vanderkelen, I., Wjiffels, S. E., Wu, T., and Zemp, M.: Heat stored in the Earth system 1960–2020: where does the energy go?, Earth System Science Data, 15, 1675–1709, https://doi.org/10.5194/essd-15-1675-2023, 2023.

von Schuckmann, K., Moreira, L., Cancet, M., Gues, F., Autret, E., Baker, J., Bricaud, C., Bourdalle-Badie, R., Castrillo, L., Cheng, L., Chevallier, F., Ciani, D., de Pascual-Collar, A., De Toma, V., Drevillon, M., Fanelli, C., Garric, G., Gehlen, M., Giesen, R., Hodges, K., Iovino, D., Jandt-Scheelke, S., Jansen, E., Juza, M., Karagali, I., Lavergne, T., Masina, S., McAdam, R., Minière, A., Morrison, H., Panteleit, T. R., Pisano, A., Pujol, M.-I., Stoffelen, A., Thual, S., Van Gennip, S., Veillard, P., Yang, C., and Zuo, H.: The state of the global ocean, State of the Planet, 4-osr8, 1–30, https://doi.org/10.5194/sp-4-osr8-1-2024, 2024.

Selivanova, J., Cipollone, A., Gonzalez, N., and Iovino, D.: Assessing the new version of the CMCC Global Ocean Reanalysis System (C-GLORS), in: EGU General Assembly 2026, EGU General Assembly 2026, EGU26-12888, https://doi.org/10.5194/egusphere-egu26-12888, 2026.

Sivareddy, S., Paul, A., Sluka, T., Ravichandran, M., and Kalnay, E.: The pre-Argo ocean reanalyses may be seriously affected by the spatial coverage of moored buoys, Scientific Reports, 7, 46685, https://doi.org/10.1038/srep46685, 2017.

Song, Y. and Forget, G.: Temperature Change in Mode Water Source Regions, Journal of Climate, https://doi.org/10.1175/jcli-d-26-0127.1, 2026.

Storto, A. and Yang, C.: Acceleration of the ocean warming from 1961 to 2022 unveiled by large-ensemble reanalyses, Nat Commun, 15, 545, https://doi.org/10.1038/s41467-024-44749-7, 2024.

https://doi.org/10.5194/egusphere-2026-6613
Preprint. Discussion started: 3 November 2026
© Author(s) 2026. CC BY 4.0 License.

Storto, A., Masina, S., and Navarra, A.: Evaluation of the CMCC eddy-permitting global ocean physical reanalysis system (C-GLORS, 1982–2012) and its assimilation components, Quarterly Journal of the Royal Meteorological Society, 142, 738–758, https://doi.org/10.1002/qj.2673, 2016.

Storto, A., Alvera-Azcárate, A., Balmaseda, M. A., Barth, A., Chevallier, M., Counillon, F., Domingues, C. M., Drevillon, M., Drillet, Y., Forget, G., Garric, G., Haines, K., Hernandez, F., Iovino, D., Jackson, L. C., Lellouche, J.-M., Masina, S., Mayer, M., Oke, P. R., Penny, S. G., Peterson, K. A., Yang, C., and Zuo, H.: Ocean Reanalyses: Recent Advances and Unsolved Challenges, Frontiers in Marine Science, 6, 418, https://doi.org/10.3389/fmars.2019.00418, 2019.

Storto, A., Cheng, L., and Yang, C.: Revisiting the 2003–18 Deep Ocean Warming through Multiplatform Analysis of the Global Energy Budget, Journal of Climate, 35, 4701–4717, https://doi.org/10.1175/jcli-d-21-0726.1, 2022.

Su, H., Zhang, H., Geng, X., Qin, T., Lu, W., and Yan, X.-H.: OPEN: A New Estimation of Global Ocean Heat Content for Upper 2000 Meters from Remote Sensing Data, Remote Sensing, 12, 2294, https://doi.org/10.3390/rs12142294, 2020.

Trenberth, K. E., Fasullo, J. T., von Schuckmann, K., and Cheng, L.: Insights into Earth's Energy Imbalance from Multiple Sources, Journal of Climate, 29, 7495–7505, https://doi.org/10.1175/jcli-d-16-0339.1, 2016.

Uotila, P., Goosse, H., Haines, K., Chevallier, M., Barthélemy, A., Bricaud, C., Carton, J., Fučkar, N., Garric, G., Iovino, D., Kauker, F., Korhonen, M., Lien, V. S., Marnela, M., Massonnet, F., Mignac, D., Peterson, K. A., Sadikni, R., Shi, L., Tietsche, S., Toyoda, T., Xie, J., and Zhang, Z.: An assessment of ten ocean reanalyses in the polar regions, Climate Dynamics, 52, 1613–1650, https://doi.org/10.1007/s00382-018-4242-z, 2019.

Wong, A. P. S., Wijffels, S. E., Riser, S. C., Pouliquen, S., Hosoda, S., Roemmich, D., Gilson, J., Johnson, G. C., Martini, K., Murphy, D. J., Scanderbeg, M., Bhaskar, T. V. S. U., Buck, J. J. H., Merceur, F., Carval, T., Maze, G., Cabanes, C., André, X., Poffa, N., Yashayaev, I., Barker, P. M., Guinehut, S.,

https://doi.org/10.5194/egusphere-2026-6613
Preprint. Discussion started: 3 November 2026
© Author(s) 2026. CC BY 4.0 License.

Belbéoch, M., Ignaszewski, M., Baringer, M. O., Schmid, C., Lyman, J. M., McTaggart, K. E., Purkey, S. G., Zilberman, N., Alkire, M. B., Swift, D., Owens, W. B., Jayne, S. R., Hersh, C., Robbins, P., West-Mack, D., Bahr, F., Yoshida, S., Sutton, P. J. H., Cancouët, R., Coatanoan, C., Dobbler, D., Juan, A. G., Gourrion, J., Kolodziejczyk, N., Bernard, V., Bourlès, B., Claustre, H., D'Ortenzio, F., Le Reste, S., Le Traon, P.-Y., Rannou, J.-P., Saout-Grit, C., Speich, S., Thierry, V., Verbrugge, N., Angel-Benavides, I. M., Klein, B., Notarstefano, G., Poulain, P.-M., Vélez-Belchí, P., Suga, T., Ando, K., Iwasaska, N., Kobayashi, T., Masuda, S., Oka, E., Sato, K., Nakamura, T., Sato, K., Takatsuki, Y., Yoshida, T., Cowley, R., Lovell, J. L., Oke, P. R., van Wijk, E. M., Carse, F., Donnelly, M., Gould, W. J., Gowers, K., King, B. A., Loch, S. G., Mowat, M., Turton, J., Rama Rao, E. P., Ravichandran, M., Freeland, H. J., Gaboury, I., Gilbert, D., Greenan, B. J. W., Ouellet, M., Ross, T., Tran, A., Dong, M., Liu, Z., Xu, J., Kang, K., Jo, H., Kim, S.-D., and Park, H.-M.: Argo Data 1999–2019: Two Million Temperature-Salinity Profiles and Subsurface Velocity Observations From a Global Array of Profiling Floats, Frontiers in Marine Science, 7, 700, https://doi.org/10.3389/fmars.2020.00700, 2020.

Xue, Y., Balmaseda, M. A., Boyer, T., Ferry, N., Good, S., Ishikawa, I., Kumar, A., Rienecker, M., Rosati, A. J., and Yin, Y.: A Comparative Analysis of Upper-Ocean Heat Content Variability from an Ensemble of Operational Ocean Reanalyses, Journal of Climate, 25, 6905–6929, https://doi.org/10.1175/jcli-d-11-00542.1, 2012.

Yang, C., Storto, A., and Masina, S.: Quantifying the effects of observational constraints and uncertainty in atmospheric forcing on historical ocean reanalyses, Climate Dynamics, 52, 3321–3342, https://doi.org/10.1007/s00382-018-4331-z, 2019.

Yang, C., Bourdallé-Badie, R., Drevillon, M., Amaya, D., Aouf, L., Aydogdu, A., Barton, B., Bell, M., Boyer, T., Blauw, A., Carton, J., Candela, T., Cossarini, G., Dabrowski, T., de Boisseson, E., de Mora, L., Fablet, R., Forget, G., Fujii, Y., Garric, G., Giunta, V., Salamon, P., Hersbach, H., Juza, M., Le Sommer, J., Martin, M., McAdam, R., Menendez Garcia, M., Morim, J., Nicolì, D., Reppucci, A., Samuelsen, A., Sauzède, R., Slivinski, L., Specq, D., Storto, A., Tuomi, L., Vandenbulcke, L., Aznar, R., Beuvier, J., Cipollone, A., Clementi, E., Di Biagio, V., Escudier, R., Giesen, R., Greiner, E., Guihou, K.,

https://doi.org/10.5194/egusphere-2026-6613
Preprint. Discussion started: 3 November 2026
© Author(s) 2026. CC BY 4.0 License.

Korabel, V., Lamouroux, J., Law Chune, S., Lellouche, J.-M., Levier, B., Lima, L., Mangin, A., Mayer, M., Melet, A., Miraglio, P., Oikonomou, C., Pfeffer, J., Renshaw, R., Ringgaard, I., Thual, S., Titaud, O., Tonani, M., van Gennip, S., von Schuckmann, K., Drillet, Y., and Le Traon, P.-Y.: Gathering Users and Developers to Shape Together the Next-Generation Ocean Reanalyses, Bulletin of the American Meteorological Society, 106, E419–E429, https://doi.org/10.1175/bams-d-24-0034.1, 2025.

Yuan, H., Cheng, L., Pan, Y., Zhang, B., Meyssignac, B., Trenberth, K. E., Zhu, Y., Song, X., Zheng, H., Bao, S., Du, J., Zhu, J., Jin, Z., Chi, X., Jiang, J., Zhang, R., Tian, Y., and Liu, N.: Six-fold reduction in ocean heat content estimate uncertainty since 1960, Nature Communications, 17, 10317, https://doi.org/10.1038/s41467-026-76436-0, 2026.

Zhang, H., Bai, X., and Wang, K.: Response of the Arctic sea ice–ocean system to meltwater perturbations based on a one-dimensional model study, Ocean Science, 19, 1649–1668, https://doi.org/10.5194/os-19-1649-2023, 2023.

Zhang, H., Storto, A., Bai, X., and Yang, C.: Quantifying the interplay of sea ice meltwater and ice–albedo feedbacks in the Arctic ice-ocean system, The Cryosphere, 19, 6807–6826, https://doi.org/10.5194/tc-19-6807-2025, 2025.

Zhu, Y., Cheng, L., Trenberth, K. E., Abraham, J. P., Speich, S., and Zhu, J.: Critical dependence of global ocean heat monitoring on the ocean observing system, Nature Climate Change, 16, 657–660, https://doi.org/10.1038/s41558-026-02661-6, 2026.

Zuo, H., Balmaseda, M. A., and Mogensen, K.: The new eddy-permitting ORAP5 ocean reanalysis: description, evaluation and uncertainties in climate signals, Climate Dynamics, 49, 791–811, https://doi.org/10.1007/s00382-015-2675-1, 2017.

Zuo, H., Balmaseda, M. A., Tietsche, S., Mogensen, K., and Mayer, M.: The ECMWF operational ensemble reanalysis–analysis system for ocean and sea ice: a description of the system and assessment, Ocean Science, 15, 779–808, https://doi.org/10.5194/os-15-779-2019, 2019.

https://doi.org/10.5194/egusphere-2026-6613
Preprint. Discussion started: 3 November 2026
© Author(s) 2026. CC BY 4.0 License.

